PHYSICAL REVIEW C, VOLUME 62, 034607

Light particle probes of expansion and temperature evolution: Coalescence model analyses of heavy ion collisions at 47*A* MeV

K. Hagel,[1] R. Wada,[1] J. Cibor,[1,2] M. Lunardon,[1,3] N. Marie,[1,4] R. Alfaro,[1] W. Shen,[5] B. Xiao,[1] Y. Zhao,[1] Z. Majka,[6] J. Li,[1]
P. Staszel,[2] B.-A. Li,[1] M. Murray,[1] T. Keutgen,[1] A. Bonasera,[1,7] and J. B. Natowitz[1]
[1]*Cyclotron Institute, Texas A&M University, College Station, Texas 77843*
[2]*Institute of Nuclear Physics, ul. Radzikowskiego 152, PL-31-342 Krakow, Poland*
[3]*Universita di Padua, Dipartimento di Fisica, Padova, Italy*
[4]*Laboratoire de Physique Corpusculaire, 14050 Caen Cedex, France*
[5]*Chinese Academy of Science, Shanghai Institute of Nuclear Research, Shanghai 201800, People's Republic of China*
[6]*Jagellonian University, M Smoluchowski Institute of Physics, PL-30059 Krakow, Poland*
[7]*Laboratori Nazionali del Sud, I-95123 Catania, Italy*

(Received 29 March 2000; published 14 August 2000)

The reactions ^{12}C+^{116}Sn, ^{22}Ne+Ag, ^{40}Ar+^{100}Mo, and ^{64}Zn+^{89}Y have been studied at 47*A* MeV projectile energy. For these reactions the most violent collisions lead to increasing amounts of fragment and light particle emission as the projectile mass increases. This is consistent with quantum molecular dynamics (QMD) model simulations of the collisions. Moving source fits to the light charged particle data have been used to gain a global view of the evolution of the particle emission. Comparisons of the multiplicities and spectra of light charged particles emitted in the reactions with the four different projectiles indicate a common emission mechanism for early emitted ejectiles even though the deposited excitation energies differ greatly. The spectra for such ejectiles can be characterized as emission in the nucleon-nucleon frame. Evidence that the ^{3}He yield is dominated by this type of emission and the role of the collision dynamics in determining the ^{3}H/^{3}He yield ratio are discussed. Self-consistent coalescence model analyses are applied to the light cluster yields, in an attempt to probe emitter source sizes and to follow the evolution of the temperatures and densities from the time of first particle emission to equilibration. These analyses exploit correlations between ejectile energy and emission time, suggested by the QMD calculations. In this analysis the degree of expansion of the emitting system is found to increase with increasing projectile mass. The double isotope yield ratio temperature drops as the system expands. Average densities as low as $0.36\rho_0$ are reached at a time near 100 fm/*c* after contact. Calorimetric methods were used to derive the mass and excitation energy of the excited nuclei which are present after preequilibrium emission. The derived masses range from 102 to 116 u and the derived excitation energies increase from 2.6 to 6.9 MeV/nucleon with increasing projectile mass. A caloric curve is derived for these expanded $A\sim110$ nuclei. This caloric curve exhibits a plateau at temperatures near 7 MeV. The plateau extends from $\sim$3.5 to 6.9 MeV/nucleon excitation energy.

PACS number(s): 25.70.Mn, 24.10.Lx

I. INTRODUCTION

In order to understand the properties of highly excited nuclei produced in heavy ion collisions it is very desirable to extract, directly from the experimental data if possible, information on the dynamical and thermodynamical evolution of the interaction region and the extent to which equilibration of various degrees of freedom, thermal, chemical, isospin, etc., is realized. If a collision produces sufficient thermal and/or compressional shock, the hot composite nucleus which results may expand to low density, cluster and disassemble [1,2]. In an ideal situation this disassembly would be that of a thermally and chemically equilibrated nucleus [3–5]. In practice the ideal state may not be reached and the final product distribution may include fragments and particles originating from nonequilibrium processes and reflecting correlations already present in the separated projectile and target nuclei [6,7]. The light particle emission which occurs during violent collisions of two heavy nuclei carries essential information on the early dynamics and on the degree of equilibration at each stage of the reaction. As a first step toward exploiting the light particle information to follow the dynamical and thermodynamical evolution of multifragmentation reactions of medium to heavy mass nuclei, we recently applied particle-fragment correlation techniques to determine the last stage yield of secondary decay particles in central collisions of ^{129}Xe with ^{124}Sn at 50*A* MeV [8]. We found that such emission from fragments accounted for 28% of the total light charged particle multiplicity. From these multiplicities we deduced an average excitation energy $\sim$3 MeV/nucleon for the primary fragments, independent of fragment mass, which provided evidence for the equilibrated nature of the disassembling system.

Our next goal has been to develop techniques which will allow us to exploit the information on early particle emission to obtain more specific information on the reaction dynamics and on the thermal evolution of multifragmenting systems produced in central collisions. To pursue this we have focused on the nucleon and light cluster emission which occurs prior to disassembly, as the system thermalizes and equilibrates. Since light cluster production in heavy ion collisions reflects the particle-particle correlations within the interaction region, detection of a cluster can be viewed as a correlation measurement of its constituent particles in a bound

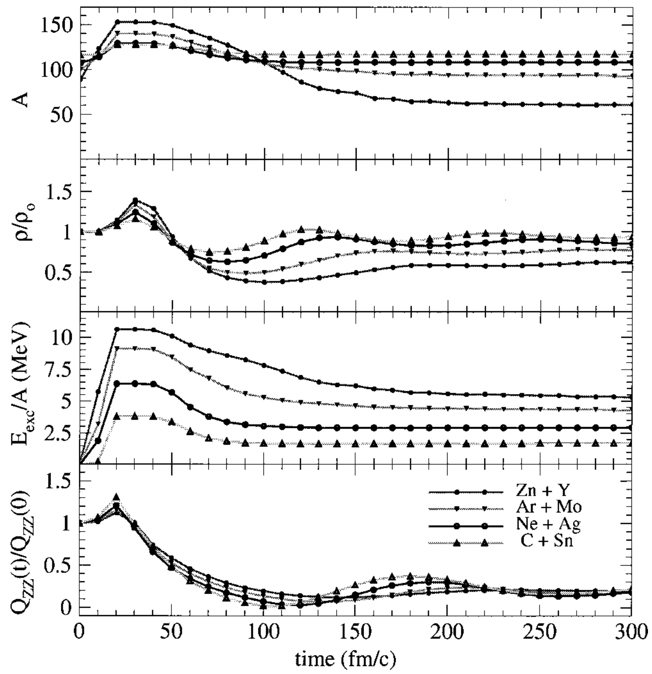

FIG. 1. CHIMERA QMD model calculations of the time evolution of the properties of the largest identifiable fragments produced in reactions induced by 47*A* MeV projectiles. From top to bottom: The mass number, the normalized density, the excitation energy per nucleon and the normalized second moment of the momentum distribution, a measure of the degree of thermal equilibration. The calculations are for an impact parameter range of 0–3 fm.

state. Therefore, measurement of emission cross sections of nucleons and light clusters together with suitable application of a coalescence ansatz [9–13] offers a means to probe the properties and evolution of the interaction region. This approach is complementary to Hanbury Brown–Twiss (HBT) measurements which are now well established in the nuclear context and have been applied in a wide range of studies [14,15]. In this paper we report on the use of coalescence model analyses of light particle emission to probe the dynamic and thermodynamic evolution of hot nuclei produced in a series of reactions between 47*A* MeV projectiles and medium mass target nuclei using a combined CsI ball-neutron–ball detection system.

A. QMD model simulations

The reactions studied were ^{12}C+^{116}Sn, ^{22}Ne+Ag, ^{40}Ar+^{100}Mo, and ^{64}Zn+^{89}Y, all at 47*A* MeV projectile energy. The choice to study this series was guided by QMD transport model calculations. Figures 1 and 2 show results of calculations carried out with the QMD code CHIMERA [16]. The calculations were carried out using standard default parameters of the CHIMERA code for a ‘‘soft’’ equation of state, with a Skyrme type interaction having an incompressibility parameter $K=200$. These parameters have previously been observed to provide a good reproduction of linear momentum transfer systematics in this energy range [17]. As indicated in the figures, the particular set of target and projectile combinations used in our experiment are predicted to lead, after preequilibrium emission of particles, to excited composite nuclei of very similar mass. The initial compression and excitation energy are predicted to increase monotonically as the projectile mass increases. The combined thermal and compressional energies, which are deposited, lead to increasing expansions of the composite nuclei.

The nuclei reach their minimum densities near 100 fm/*c*, at which point thermal equilibrium appears to be essentially established. Prior to the time that global thermal equilibrium is achieved the preequilibrium particle emission removes significant amounts of both mass and energy from the expanding composite nuclei. As seen in Fig. 1, at the time of maximum expansion, the excited composite nuclei produced in the different collisions are predicted to have masses $A\sim 110$, calculated excitation energies which range from 3–8 MeV/nucleon and densities which range from slightly below normal density, $0.8\rho_0$, to $\sim 0.4\rho_0$. For the heavier projectiles, the calculations with a soft (incompressibility, $K=200$ MeV) equation of state suggest that the system enters into the spinodal region of mechanical instability (see Refs. [18–20], and references therein). Increasing multifragment production is predicted as the projectile mass increases. This increase is indeed manifested in our experimental results as seen below.

B. Correlation of kinetic energy and time

An inspection of the calculated energy spectra of the emitted particles over the 50 to 100 fm/*c* time range reveals that there is a monotonic decrease of the average kinetic energy with increasing time. This is depicted for proton emission in the ^{12}C+^{116}Sn and ^{64}Zn+^{89}Y collisions in Fig. 2. After 100 fm/*c*, the calculated average ejectile kinetic energies change much more slowly. This early evolution of the kinetic energy is, of course, governed by nucleon collisions and it is worth noting that much simpler formulations of nucleon scattering in a nucleus also predict both the initial rapid ejectile energy decrease with time and the capture of nucleons (and hence thermalization) after very few collisions [21–23]. Such a correlation between energy and emission time has, in fact, been clearly demonstrated in reactions induced by ^{40}Ar projectile energies of 25 MeV/nucleon [24] and 34 MeV/nucleon [25] by employing light particle correlation measurements to determine the mean times for emission of hydrogen ejectiles as a function of particle velocity.

Thus both theoretical models and experiments suggest that the relationship between emission time and particle energy might be exploited to follow the time evolution of the system in more detail than has been attempted in previous works which have generally limited themselves to a relatively crude separation of the particle emission into two classes, i.e., preequilibrium and equilibrium emission. Specifically, if light particle energies are well correlated with emission times, and evaporative or secondary emission contributions contribute to the spectra primarily at the lower kinetic energies, yields of higher energy particles may be relatively uncontaminated by later emission processes. Analyses of the higher energy parts of the particle energy spectra can then be used to probe the early stage properties

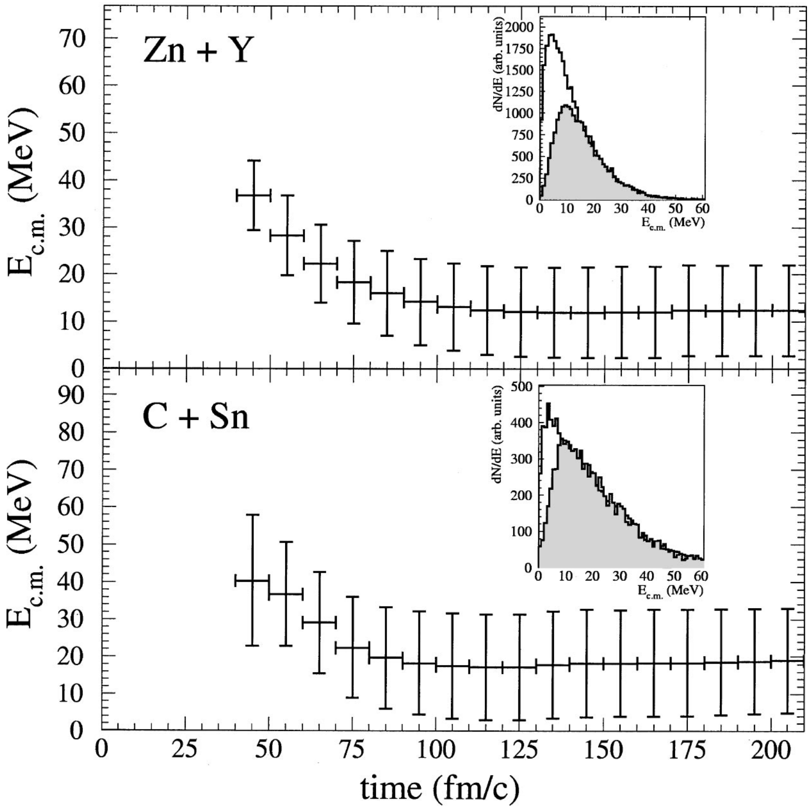

FIG. 2. CHIMERA QMD model calculations of the time evolution of the average kinetic energies of protons emitted in the 0–3 fm impact parameter collisions of ^{64}Zn+^{89}Y (top) and ^{12}C + ^{116}Sn (bottom) at 47A MeV. The inserts show the spectral distributions at 80 (shaded) and 120 (unshaded) fm/c.

of the system. Related suggestions have previously been made in the context of temperature determinations [26–32]. In thermal equilibrium models the cooling of the system leads to progressively softer particle spectra. Assuming such an equilibrium thermal evolution several workers have incorporated techniques based on analysis of the higher energy particles into evaluations of slope temperatures [26,27] and, more recently, double isotope ratio temperatures [29]. The possible effects of emission time differences on temperature determinations has also received some attention recently [30–32].

Guided by these considerations we have carried out analyses of nucleon and light cluster emission as a function of particle velocity, basing our approach on coalescence model techniques [9–13]. This paper presents the results of such analyses and discusses the implications of these results for dynamics studies and caloric curve determinations. Sections II and III detail experimental procedures and results which characterize the reaction systems. Section IV discusses moving source fits and calorimetry. Section V treats the coalescence model analyses which we have applied. The work is summarized in Sec. VI. Brief reports on some of these results have appeared previously [33].

II. EXPERIMENTAL PROCEDURES

The combined TAMU CsI Ball-Neutron Ball detection system was used to detect light charged particles, fragments and neutrons emitted in reactions induced by 47A MeV beams of ^{12}C, ^{22}Ne, ^{40}Ar, and ^{89}Y extracted from the TAMU K500 Superconducting Cyclotron. Targets of 685 μg/cm^2 ^{116}Sn, 538 μg/cm^2 Ag, 526 μg/cm^2 ^{100}Mo, and 1.28 mg/cm^2 ^{89}Y were employed. The CsI Ball consisted of 96 ionization chamber-CsI telescopes in seven rings and spanned an angular range Θ_L of 20–170 °. One telescope in each CsI ring also had a 150 micron transmission-mount Si detector between the IC and CsI detectors. The total solid angle covered by the CsI ball was 86% of 4π. Forward hodoscopes combining plastic-CsI and Si-CsI detectors were also employed at smaller angles but with relatively low solid angle coverage. Most of the data discussed in this paper came from the CsI ball detectors. Energy spectra and angular distributions of identified p,d,t, ^{3}He, ^{4}He and of elements of $3<Z<14$ were obtained. The identification of p,d,t, ^{3}He, and ^{4}He in the CsI detectors was carried out using pulse shape identification techniques. Calibration of the Si detectors was performed with standard alpha sources and a linear pulser. The CsI detectors were calibrated using alpha sources, the energy losses in the Si for $Z=1$ and 2 particles and the punch through points for both Si and CsI detectors. In the analysis the calibration for the Si-CsI detector in each ring was first determined and all other detectors in the same ring were then calibrated relative to that standard detector telescope.

The geometric efficiency of the CsI ball is about 86% of 4π. Realized efficiencies for charged particle detection in the CsI ball and neutrons in the neutron ball decrease slowly with increasing projectile mass, reflecting the increased kinematic focusing of ejectiles into the more forward direction. In addition to the geometric decrease, the neutron ball intrinsic efficiency further decreases as the neutron laboratory energy increases with increasing velocity and temperature of the neutron source [34]. Charged particle multiplicities were

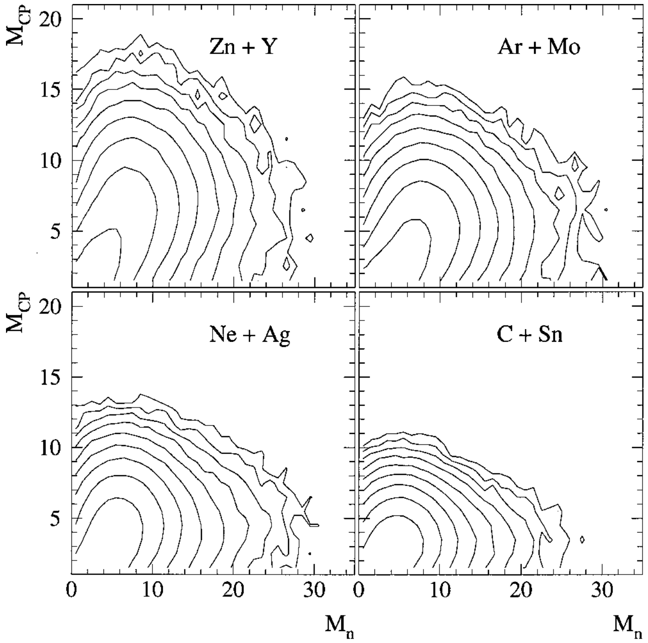

FIG. 3. Plots of detected charged particle multiplicity vs detected neutron multiplicity for the four reactions studied. No corrections have been made for efficiency. Average corrections for background contributions to the neutrons have been made. Each contour indicates an increase in intensity of a factor of 3.

obtained by first correcting observed spectra for geometric efficiencies of the individual detectors and then using source fitting techniques, described below, to determine total yields. Neutron multiplicities were determined from average, background corrected, detected neutron numbers for the events selected. For our neutron calorimeter a valid correction of the neutron number for background contributions is possible only on the average and not on event by event basis. Introduction of the CsI ball into the neutron ball [34] required opening the ball segments and accepting a reduced neutron efficiency. The efficiency curve of the neutron ball in its open configuration was determined relative to the normal configuration by first measuring the efficiency for ^{252}Cf neutrons and then by comparisons of the measured neutron numbers for ^{64}Zn+^{197}Au at 37 and 47*A* MeV with previous results for ^{63}Cu+^{197}Au reactions at 35*A* MeV taken with the neutron ball in its normal closed configuration [35]. The resultant efficiencies were about one half of those measured in the normal configuration.

III. REACTION SYSTEM CHARACTERIZATION

Various experimental observables may be employed to characterize the four systems studied and illustrate interesting similarities and differences among them. For example, in Fig. 3 we present two-dimensional arrays depicting the detected correlation between charged particle multiplicity and neutron multiplicity. No corrections for efficiency have been made. In each case, although there are significant fluctuations reflecting both the competition between decay modes and the detection efficiencies, we see a distinct correlation in which increasing charged particle multiplicity is associated with increasing neutron multiplicity. As the projectile mass and total energy increases both distributions extend to larger multiplicities. These correlations provide a means for selecting the most violent collisions. For the data discussed in this paper violent events corresponding to the 10% of the events having the highest charged particle multiplicities were selected for detailed analysis.

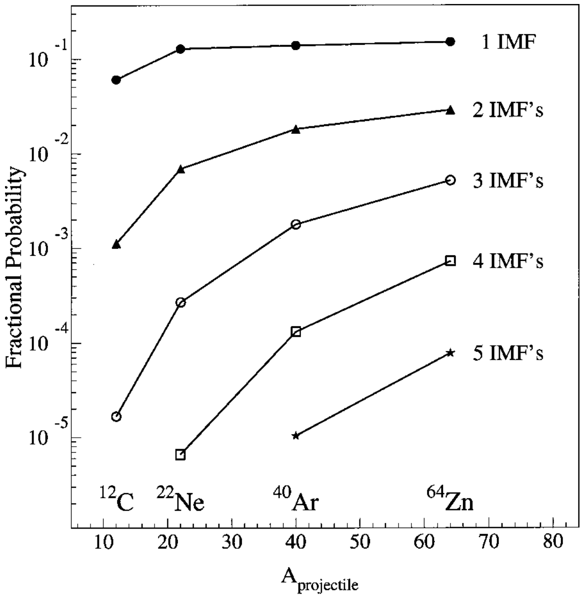

FIG. 4. Experimental fractional probability for the detection of events with specified numbers of intermediate mass fragments in the violent collisions (see text). The fractional probabilities for detection of 1, 2, 3, 4, or 5 IMF's, represented respectively by filled circular points, filled triangles, open circles, open squares and stars, are plotted as a function of projectile mass. Lines are to guide the eye.

For these selected events multifragment emission is observed to become increasingly more probable as the projectile mass increases, in agreement with the QMD model predictions. This is shown clearly in Fig. 4 where the fractional probabilities per event for producing a given number of intermediate mass fragments of $3<Z<14$ are plotted for the four different reaction systems.

Figure 5 contains invariant velocity plots of the intensities of light charged particles emitted in the reactions studied as a function of their parallel and transverse velocities in the laboratory frame. To construct this plot the histogrammed data from the discrete detector rings were smoothed by random assignment of the position for a particle detected in a given detector, constrained by the observed angular distribution. These plots reveal very strong similarities for the different systems. As seen in the following section it is possible to parametrize such emission as reflecting, in all cases, a fairly intense isotropic emission of particles from a hypothetical source which has a velocity close to one half of the projectile velocity, i.e., the velocity of the nucleon-nucleon (*NN*) collision frame. Emission from such an apparent source of velocity near one half of the beam velocity has previously been found to be characteristic of nonequilibrium emission in this projectile energy range (see Refs. [12,27],

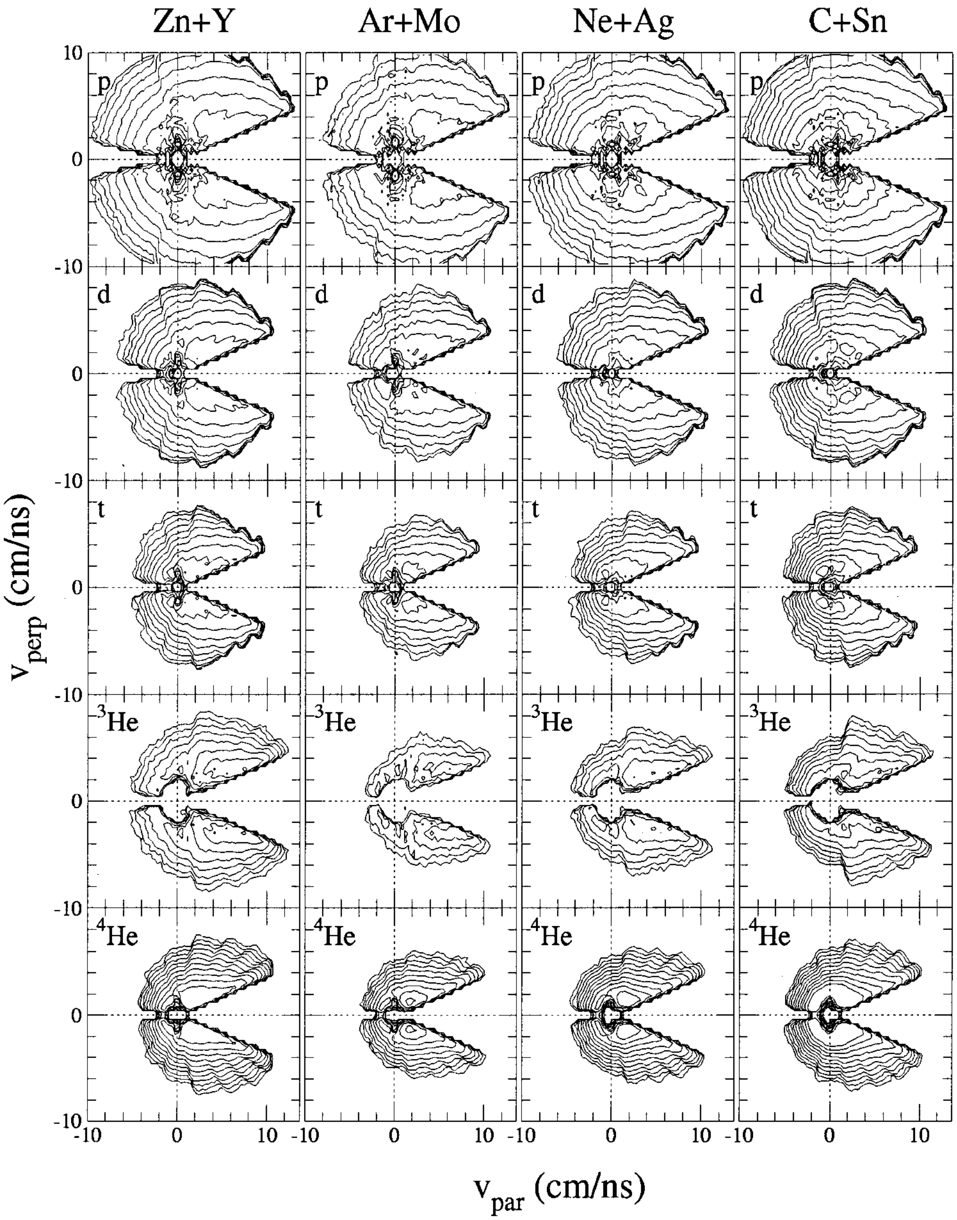

FIG. 5. Invariant velocity plots for *p, d, t,* ^{3}He, and ^{4}He detected in violent collisions for the reactions ^{12}C+^{116}Sn, ^{22}Ne+Ag, ^{40}Ar+^{100}Mo, and ^{64}Zn+^{89}Y. Each contour indicates an increase in intensity of a factor of 2.

and references therein). For ^{64}Zn+^{89}Y this source is so dominant that emission from the targetlike source is only weakly evident. For progressively lighter projectiles the emission from the targetlike source is progressively easier to see, as the relative intensity of emission from the intermediate source becomes weaker. For ^{12}C+^{116}Sn the emission from the targetlike source is easily apparent.

To emphasize the similarities among the energy spectra in the different reactions, we present in Fig. 6, comparisons of the (arbitrarily normalized) kinetic energy spectra for p,d,t, ^{3}He, ^{4}He detected in ring 3 of the CsI ball detector. This ring subtended an angular range of 38–52 ° in the laboratory. This figure shows clearly that the higher energy tails of the spectra for each individual ejectile type are essentially identical for each system studied. This argues strongly for a similar mechanism of production for these higher energy ejectiles in the different systems. The slopes of the high energy tails for p,d,t and ^{3}He emission are quite similar to each other while the slope characterizing the high energy region of the α particle spectra is somewhat softer.

At lower kinetic energies the spectra for the different systems show larger deviations from each other. There is also evidence, at least for the lighter projectiles of low-energy peaks typical of evaporation spectra. The ^{3}He spectra show somewhat less evidence for this latter feature. That ^{3}He energy spectra are often quite different from those of other light composite particles has been known for some time [36–39]. Recently it has been suggested, based on an expanding emitting source model, that this reflects the strong weighting of the probability of thermal ^{3}He evaporation towards early times in the emission cascade and a very low emission probability at later stages [31,32,39]. Our results support the arguments that ^{3}He is predominately emitted in the early stages of the reaction [33]. However, for all systems studied the ^{3}He spectra exhibit strong similarities even though the deposited excitation energies differ greatly. This, and the fact

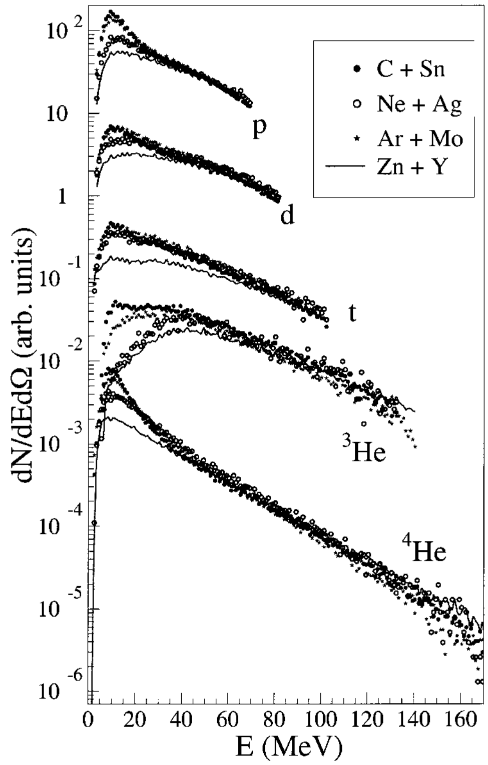

FIG. 6. Laboratory kinetic energy spectra of light particles emitted at $\Theta_{\mathrm{lab}} = 38$–$52°$ for the four reactions studied. Event selection is the same as for Fig. 5. The spectra are arbitrarily normalized in the high energy region.

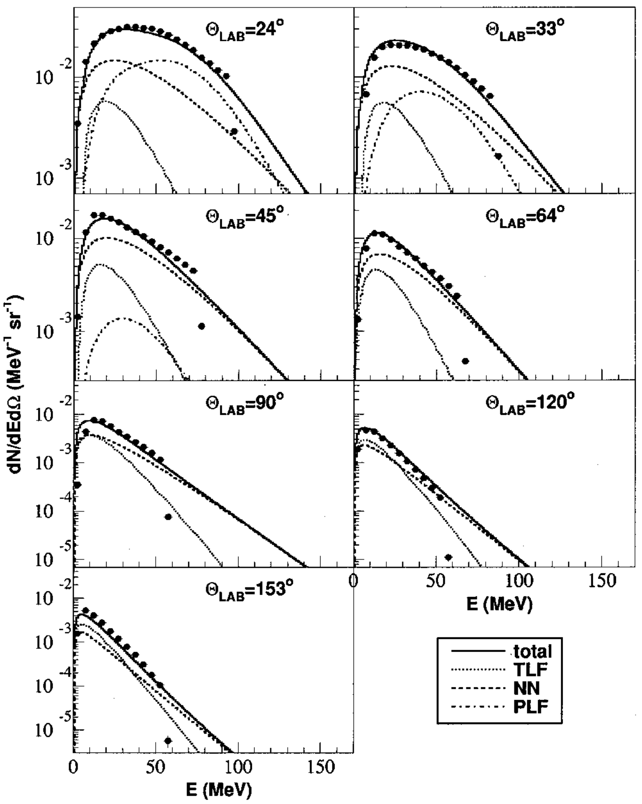

FIG. 7. Source fit representations of the laboratory kinetic energy spectra of protons emitted in violent collisions of ^{64}Zn+^{89}Y for seven angular ranges from 20° to 170°. The solid points represent the data. Contributions from the PLF, *NN*, and TLF sources are respectively represented by dot-dashed, dashed, and dotted lines. The summed contributions are represented by solid lines.

that the bulk of the ^{3}He emission appears to be from a source having a velocity close to the velocity of the nucleon-nucleon collision frame, independent of system, indicates that dynamics is particularly important in the ^{3}He emission. Thermal evaporation, early or late, appears to account for only a small fraction of the ^{3}He observed in this work. These observations emphasize the importance of understanding the dynamic evolution of the system and the emission time relationships for different species if one wishes to characterize the thermodynamic properties of well-defined sources.

IV. MOVING SOURCE ANALYSIS

A common technique to characterize light particle emission in this energy range has been to fit the observed spectra assuming contributions from three sources, a projectilelike fragment (PLF) source, an intermediate velocity (*NN*) source, and a targetlike fragment (TLF) source [12,27,40,41]. We have performed such an analysis. However, given the continuous dynamic evolution of the system, source fits should be considered as providing only a schematic picture of the emission process [25,41]. We have employed them to estimate the multiplicities and energy emission at each stage of the reaction. To follow the time evolution of the system in more detail a more sophisticated analysis of the particle emission is necessary. Figures 7 and 8 provide examples of the results of global moving source fits to the proton and α particle data for the ^{64}Zn+^{89}Y reaction. Except for the most forward detector rings the data for this reaction, and for the other systems, are dominated by particles associated with the *NN* and TLF sources and a reasonable reproduction of the observed spectra is achieved.

In this analysis the source velocities, emission barriers, temperatures, and particle multiplicities for the three different sources were searched for. We emphasize that the event selection is on the most violent and presumably more central collisions. In the fitting process, which assumes isotopic emission and a Maxwellian spectral shape in the particular source frame considered, accounting for forward emitted particles with projectilelike velocities requires the PLF source. We consider these particles to be of preequilibrium emission origin and not to be evaporated from a fragment.

In Fig. 9 the source fit parameters derived for the *NN* and TLF sources are presented. Several features of these parameters are worth noting: For the *NN* source the multiplicities of light charged ejectiles increase smoothly with projectile size. Temperatures and source velocities vary only slightly with projectile mass. The *NN* source velocities are very close to 50% of the beam velocity as seen in many other studies. The slope temperatures of 16 to 18 MeV for p,d,t and ^{3}He are quite similar and also similar to earlier reported values for such projectile energies [27,40]. As already noted in the discussion of Fig. 6 the slope temperatures for ^{4}He are

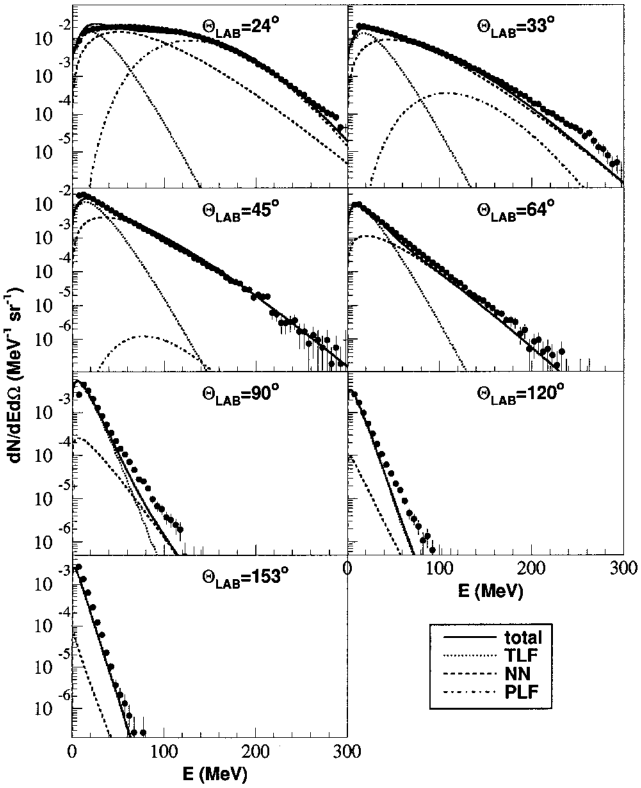

FIG. 8. Source fit representations of the laboratory kinetic energy spectra of α particles emitted in violent collisions of ^{64}Zn $+{}^{89}$Y for seven angular ranges from 20 ° to 170°. The solid points represent the data. Contributions from the PLF, *NN*, and TLF sources are, respectively, represented by dot-dashed, dashed, and dotted lines. The summed contributions are represented by solid lines.

somewhat lower. The barrier parameters, poorly defined in these fits, are somewhat lower. The ^{3}He barriers are notably higher than the barriers for the other particles, reflecting the quite different shapes of the ^{3}He spectra as seen in Fig. 6.

For the TLF source the multiplicities of light charged ejectiles show smaller variations with projectile size. Slope temperatures and source velocities increase monotonically with projectile mass. The TLF source velocities are roughly consistent with the expectations based on existing linear momentum transfer systematics [42,43]. For a given reaction system, the slope temperatures for the different ejectiles are quite similar.

TLF source properties. The masses and excitation energies of the hot nuclei which remain after the early (PLF and *NN* source) emission have been determined. The masses were obtained by subtracting the mass removed by projectile-source and intermediate source particles from the total entrance channel mass. The multiplicities of charged particles used for this determination were those determined from the source fits, i.e., integrated over 4π. The neutron multiplicities from the PLF and *NN* sources were estimated from proton multiplicities, the former from the N/Z ratio of the projectile, the latter from the observed $t/{}^3$He ratio for the *NN* source.

Excitation energies remaining in the TLF source were determined using calorimetric techniques. For this purpose we combined the information on the multiplicities and kinetic energies of light charged particles and intermediate mass fragments associated with the TLF source and also the neutron multiplicity information from the neutron ball. Since the neutron energies were not measured we assigned an average neutron emission energy, assuming volume emission, of $3T/2$ where $T=4$ MeV for the C + Sn reaction and 4.7 MeV for the other systems. These estimates were made by taking into consideration that the double isotope yield ratio temperatures discussed below are initial temperatures and the neutron spectra are characterized by an average temperature over the long TLF neutron deexcitation cascade. Combining this information we calculated the primary TLF excitation energy as

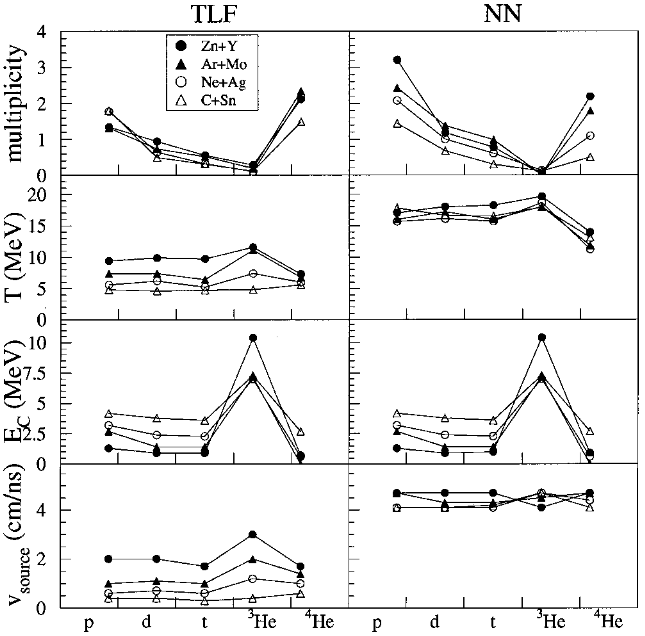

FIG. 9. Source fit parameters for the *NN* source (right) and the TLF source (left). From top to bottom, particle multiplicity, slope temperatures, Coulomb barriers, and source velocities. Symbols identify the different reactions; ^{12}C$+{}^{116}$Sn (open triangles), ^{22}Ne+Ag (open circles), ^{40}Ar$+{}^{100}$Mo (filled triangles), and ^{64}Zn $+{}^{89}$Y (filled circles). For the fits the Coulomb barriers were assumed to be the same for the two sources.

$$E^{\star}=\sum_i \overline{M}_{CP}(i)\overline{E}_{CP}(i)+\overline{M}_n\overline{E}_n+Q+E_{\gamma}, \qquad (1)$$

where the sum extends over charged particle type i, $\overline{M}_c p(i)$, $\overline{M}_n$ are average multiplicities of charged particles and neutrons, $E_c p(i)$, E_n are their average kinetic energies, $\overline{E}_\gamma$ is the energy in γ rays as (estimated 10 MeV) and Q is the Q value for the observed deexcitation starting from the primary TLF and assuming $A=2Z$ for IMF's.

We take the derived excitation energy to be that of the equilibrated expanded system at the time corresponding to the latest particle emission associated with the intermediate source and thus appropriate to the temperature determined at that time. The derived excitation energies are 2.6 MeV/nucleon for ^{12}C+^{116}Sn, 3.9 MeV/nucleon for ^{22}Ne+Ag, 5.6 MeV/nucleon for ^{40}Ar+^{100}Mo, and 6.9 MeV/nucleon for ^{64}Zn+^{89}Y with the uncertainties of $\sim 10\%$. Except for the ^{12}C induced reaction these values obtained from calorimetry are within 10% of estimates which can be made by assuming that missing mass continues forward with the beam velocity, deriving the fractional linear momentum transfer from the TLF source velocities found in the three-source fits and using this fractional transfer to calculate an excitation energy [26,27]. For the ^{12}C+^{116}Sn case, where the TLF velocity is low, the error in the derived source velocity and the corresponding difference in derived excitation energy is significantly larger than for the other systems.

V. COALESCENCE MODEL ANALYSES

We have applied coalescence model analyses in order to exploit the particle emission information to derive more specific information on the dynamic evolution of the collision. A number of previous experiments have demonstrated the utility of coalescence models to probe system sizes over a wide range of energies [9–13,44–47]. In such models the momentum space densities of ejected light composite particles with Z protons and N neutrons are directly related to the momentum space densities of neutrons and protons,

$$\gamma \frac{d^3 N_{Z,N}}{dK^3} = \left(\frac{2s+1}{2^A}\right)\frac{1}{N!Z!}\left(\frac{4\pi}{3}P_0^3\right)^{A-1} \times \left(\gamma \frac{d^3 N_p}{dK^3}\right)^Z \left(\gamma \frac{d^3 N_n}{dK^3}\right)^N, \tag{2}$$

where $N_{(Z,N)}$, N_p, and N_n represent the numbers of clusters, protons, and neutrons, respectively, K is the momentum, and γ is the Lorentz factor.

Thus the phase space correlations which lead to cluster formation may be parametrized in terms of the momentum space volume within which the correlations exist [9–13,22]. This momentum space volume is normally assumed to be spherical with a radius of P_0. Under suitable conditions, extraction of P_0 provides information on the space-time correlations analogous to that obtained in particle-particle correlation measurements.

Below we present the results of coalescence model analyses for the four different systems studied. Because our goal was to derive information on the time evolution of the emitting system, our analysis was not limited to determining an average P_0 value appropriate to the higher energy portions of the particle spectra, as is common in previous work. Instead, for d, t, ^{3}He, and ^{4}He, results are presented as a function of V_{surf}, the velocity of the emerging particle at the nuclear surface, prior to Coulomb acceleration. The decision to follow this procedure is based upon the considerations discussed in the introduction to this paper where it is pointed out that both transport model simulations and experimental particle-particle HBT studies indicate a strong correlation between emission time and ejectile kinetic energy in the early phases of a reaction.

To calibrate the timescale associated with our data we have derived the relationship between emission time of the particles detected and their average energies using the results of the QMD transport model calculations. Cast in terms of time vs V_{surf} this indicates that average emission times increasing from $\sim 80-\sim 105$ fm/c are sampled as V_{surf} decreases from 7 to 4 cm/ns and leads to the time-scales presented later at the tops of Figs. 12–16. The model calculations described in Sec. I indicate that the system is essentially thermally equilibrated near 105 fm/c when V_{surf} has dropped to 4 cm/ns.

A. Information content of P_0

In the following we report on the use of two different models, the density matrix formalism of Sato and Yazaki [11] and the thermal model of Mekjian [10], to extract nuclear size information for evolving systems using P_0 determinations. In the first model neither chemical nor thermal equilibrium is assumed and the radius of the emitted cluster is explicitly taken into account. In the second model chemical and thermal equilibrium are assumed. Even though the assumptions are quite different, the very similar formal structures of coalescence models in both nonequilibrium and equilibrium conditions [9] suggests that these models may provide a natural vehicle for following the time evolution of light composite particle emission from the first emission of such particles through freeze-out.

In both the coalescence model literature and in recent transport model literature a variety of assumptions have been made regarding the actual information content of the coalescence radius, P_0 and its relationship to the properties of the emitting system and/or the properties of the emitted cluster. To clarify the utility of the coalescence approach to probe system size evolution we have recently applied coalescence model analyses to simulations of nuclear expansion [48], carried out with the well-defined classical molecular dynamics model of Belkacem *et al.* [49]. Some of the essential results of that analysis are summarized in Figs. 11 and 12 for simulations of expanding uncharged drops. It is shown in Ref. [48] that the addition of Coulomb interactions makes some small modifications but does not change the basic picture presented here.

In Fig. 10 values of P_0 derived for ‘‘deuteron’’ (a bound state of two uncharged particles in the model) emission from three different expanding systems initially consisting of 20, 50, or 100 ‘‘nucleons’’ are presented. The initial temperature in each system was 5 MeV. For the interaction used $T = 5$ MeV is well above the critical temperature for this system [49] and the system expands rapidly to low density, cooling as it does so. In Fig. 10(a) the derived values of P_0 are plotted as a function of scaled velocity v/v_T for a given particle, where $v_T = (4\ \mathrm{T/m})^{1/2}$. First we note that the absolute values of P_0 decrease with system size as is to be expected if P_0 is inversely related to the size of the system. Secondly we see that P_0 decreases as v/v_T decreases as

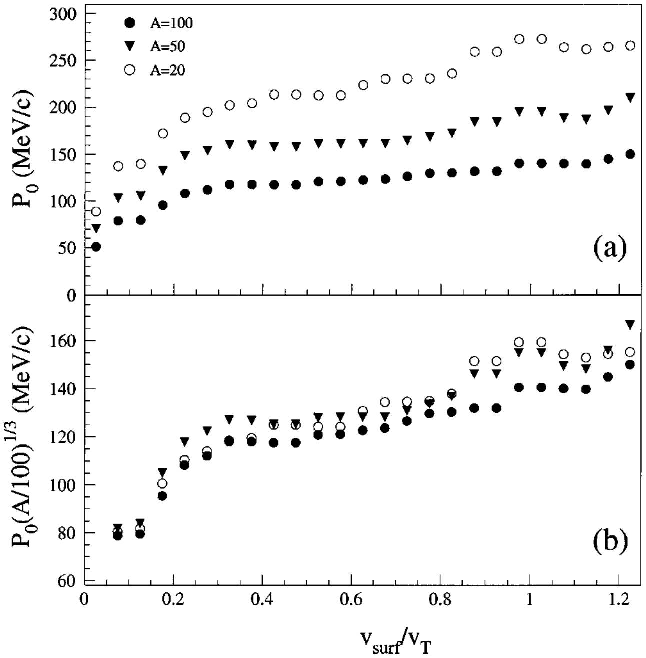

FIG. 10. CMD model calculated coalescence parameters, P_0 (top) and the scaled values of P_0 (bottom) are presented for ''deuterons'' emitted from systems with an initial temperature of 5 MeV and $A=20$, 50, or 100. Results are presented as a function of scaled thermal velocity (see text).

should be expected if the ejectile velocities decrease as the expanding system cools. The relative variations of P_0 with v/v_T for the three different systems are quite similar. That, in fact these values of P_0 scale with $A^{1/3}$ of the emitting system is confirmed in Fig. 10(b) where all values for a particular value of v/v_T in Fig. 10(a) are normalized to the corresponding value for $A=100$. Since the radius of the system may be expressed as $r_0A^{1/3}$, the decreasing value of P_0 tracks the increase in radius.

To further explore the time relationships inherent in these results we present in Figs. 11(a) and 11(b) two additional correlations derived from the simulation. In Fig. 11(a) values of P_0 as a function v/v_T of for deuterons emitted during the first 100 fm/c of the expansion are compared to the values obtained from the final deuteron spectra, representing the entire time evolution. This figure clearly demonstrates that the particles with the highest values of P_0 are emitted at the beginning of the expansion. Isolation of this contribution to the spectrum allows a measurement of the size at early time. In Fig. 11(b) we plot, as a function of time, the average neutron-proton separation distances for nucleons which eventually form deuterons. This is done for two different deuteron kinetic energy ranges. Deuterons with kinetic energies greater than 30 MeV, well above the spectral average, are formed from nucleons initially quite close to each other. Preexisting correlations in the projectile or target might be very important for such deuterons. Deuterons with kinetic energies less than 30 MeV are more likely formed from nucleons which are initially very far apart but find each other. During the time required for that, thermal and chemical equilibrium might be achieved.

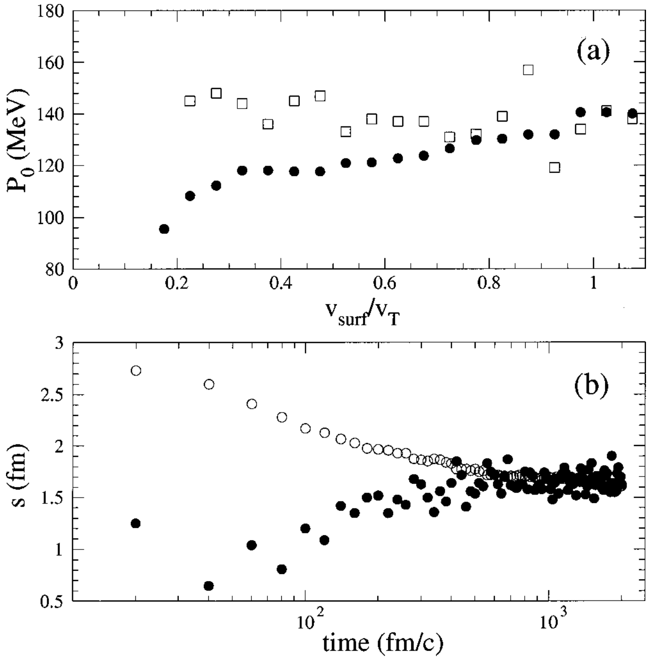

FIG. 11. Top: The coalescence parameter $P0$ calculated for ''deuteron'' emission from a system with $T=5$ MeV and $A=100$, using the CMD model. Values are shown for deuterons emitted over two different time periods, up to 100 fm/c (open squares), and up to 3000 fm/c (filled circles). In the latter case the cluster yields have reached their asymptotic values. Bottom: Average neutron-proton separation distances for nucleons which eventually form deuterons are shown for two different deuteron kinetic energy ranges. Deuterons with kinetic energies greater than 30 MeV (filled circles) and deuterons with kinetic energies less than 30 MeV (open circles).

B. Coalescence at intermediate energies

The coalescence approach has been most often applied at relativistic energies where several simplifying assumptions can be made. At intermediate energies these assumptions may not be acceptable. For example, while Coulomb forces are typically ignored at relativistic energies, Awes *et al.* [12] have shown that they must be taken into account in the energy range which is considered here. Therefore, to determine the coalescence parameter P_0 from our data we have followed the Coulomb corrected coalescence model formalism of Awes *et al.* [12]. In the laboratory frame the derived relationship between the observed cluster and proton differential cross sections is

$$\frac{d^2N(Z,N,E_A)}{dE_A d\Omega}=R_{np}^N\frac{A^{-1}}{N!Z!}\left(\frac{\frac{4}{3}\pi P_0^3}{[2m^3(E-E_c)]^{1/2}}\right)^{A-1}\times\left(\frac{d^2N(1,0,E)}{dEd\Omega}\right)^A, \tag{3}$$

where the double differential multiplicity for a cluster of mass number A containing Z protons and N neutrons and having a Coulomb-corrected energy E_A, is related to the proton double differential multiplicity at the same Coulomb corrected energy per nucleon $E-E_C$, where E_C is the Coulomb barrier for proton emission and $R_{np}^N=[(N_t+N_p)/(Z_t+Z_p)]^N$ is the invariant coalescence factor.

Certain approximations commonly employed in determining P_0 have restricted many earlier coalescence model analyses to providing only qualitative or semiquantitative information. These approximations must be avoided if quantitative information is to be derived. For example, as indicated by Eq. (2), a strict quantitative application of the coalescence model requires knowledge of cluster, neutron and proton differential cross sections with proper absolute normalizations. Many past applications have used only average normalizations, relating the observed inclusive yields to the total reaction cross section [9,12,45,46]. In this work absolute measured multiplicities for a particular class of selected violent events are employed.

Also, in Eq. (3) N_p, N_t, Z_p, and Z_t enter the equation because measurements which include neutron information are relatively rare and it has typically been assumed, in most coalescence model analyses, that the neutron energy spectra are identical in shape to the Coulomb corrected proton spectra and that the neutron yields are simply N/Z times the proton yields, where N/Z is the neutron to proton ratio in the composite system [9,11,12,46]. In this work, also, the neutron spectra are not measured. However, since within the framework of the coalescence model the yield ratios of two isotopes which differ by one neutron are essentially determined by the effective N/Z ratio in the coalescence volume. We have used values derived directly from the observed triton to ^{3}He yield ratio to determine the N/Z ratio used in this analysis. This use of this ''effective'' N/Z ratio is a self-consistent approach but may mean that some actual differences in neutron and proton spectra are absorbed into this ratio [48].

It should be noted that in nonequilibrium coalescence models the cluster yields are related to primary nucleon yields while in equilibrium coalescence models the cluster yields are related to observed nucleon yields [9]. As the system evolves, there may in fact be a shift from a predominately nonequilibrium to an equilibrium coalescence mechanism. In this work P_0 was determined using the observed proton yields. This choice is at least consistent with the apparent successes of statistical models which assume the existence of equilibrium or near-equilibrium conditions in hot expanding nuclei [3–5].

A number of previous works do, in fact, suggest that, rather than being related to ''primary'' nucleon yields, as expected in nonequilibrium coalescence models, the cluster yields are related to observed nucleon yields [9]. The reason for this is perhaps to be found in the results of transport model calculations which indicate a rapid equilibration of the emitting system [6,16,18,21]. For our systems at the calculated time of first particle emission, ∼50 fm/*c* as seen in Fig. 1, the nucleon momentum distribution, though not completely randomized in direction, is rapidly approaching that condition.

C. Determination of P_0

For the coalescence model analysis we have selected the data in ring 3 of the CsI ball detector. This ring covered an angular range of $\Theta_{\rm lab}=38°-52°$. Inspection of the invariant velocity plots constructed for each ejectile and each system, shown in Fig. 5, as well as of the results of the three-source fit analyses such as that presented in Figs. 7 and 8 indicates that this selection of angular range minimizes contributions from secondary evaporative decay of projectilelike or targetlike sources.

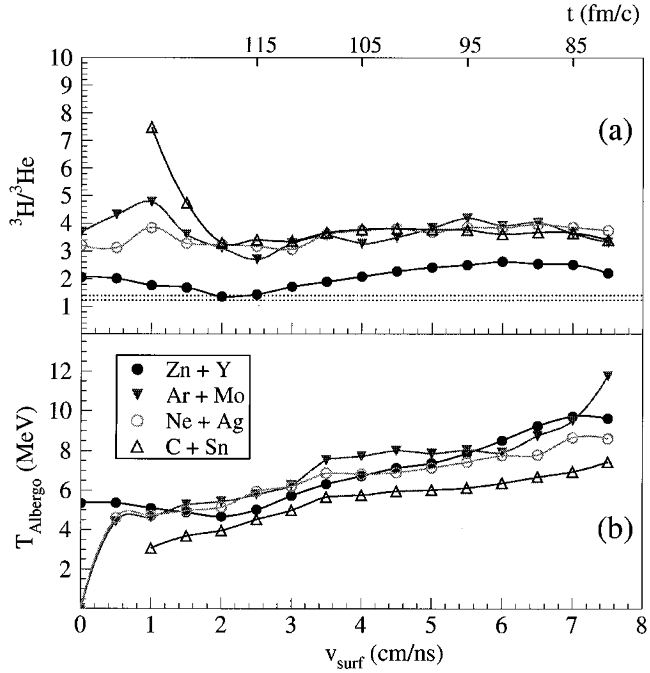

FIG. 12. Experimental ratios of ^{3}H to ^{3}He emission yields (top) and double isotope yield ratio temperatures (bottom) as a function of Coulomb-corrected surface velocity. Data below ∼4 cm/ns may have residual contributions from statistical evaporation. The horizontal bar in the top portion indicates the range of composite nucleus N/Z values for the systems studied. Time scales derived from CHIMERA QMD model calculations are indicated at the top of the figure.

D. *t*/^{3}He ratios

As indicated by Eq. (3) the coalescence model yield ratios of two isotopes which differ by one neutron are essentially determined by the ratio of ''free nucleons'' in the coalescence volume. Figure 12(a) shows measured values of the $t/^3$He ratio as a function of $V_{\rm surf}$. These ratios, closely allied to the density ratios for free nucleons, are significantly higher than the N/Z ratios in the composite systems. The range of the latter is indicated by the two dotted lines in the figure. This is consistent with results obtained by Albergo *et al.* [28] who often deduce significant free neutron excesses based on integrated yields observed in a variety of early intermediate energy experiments. Other recent work also results in large N/Z ratios [50,51]. It has been suggested that such observations provide evidence for a distillation leading to a nucleon vapor which is enriched in neutrons relative to a coexisting nuclear liquid in accordance with predictions of several recent theoretical studies [52,53]. While such a distillation process is appealing it may be that the enrichment is dynamically driven. Bonasera and Bertsch [54] have previously proposed a simple model to estimate the yield ratio for like mass species of different charge which become unbound in the collision of two heavy ions. The ratio is derived from the change in chemical potential which occurs when the two separated nuclei merge. It is argued in Ref. [54] that this change is essentially due to the difference in neutron and proton chemical potentials which results from the collision and that this difference is dominated by the Coulomb energy contributions. Generalizing that approach to emission of ^{3}H and ^{3}He clusters of the same surface velocity in asymmetric collisions, and assuming that the initial collision leads to a composite system with $Z=\varrho ZP+Z_T$ and $A=\varrho A_P+A_T$ where ϱ is the fractional momentum transfer, Z_P and Z_T are the projectile and target atomic numbers, and A_P and A_T are the projectile and target mass numbers, leads to

$$\Delta\mu\left(\frac{^3\mathrm{H}}{^3\mathrm{He}}\right)=\frac{(\rho Z_p+Z_t)e^2}{r_0\left[(\rho A_p+A_t)^{1/3}-\frac{1}{2}(Z_p/A_p^{1/3})+(Z_t/A_t^{1/3})\right]}$$

and

$$R\left(\frac{^3\mathrm{H}}{^3\mathrm{He}}\right)=\exp\left(\frac{2\Delta\mu(^3\mathrm{H}/^3\mathrm{He})}{T}\right), \tag{4}$$

where $\Delta\mu(^3\mathrm{H}/^3\mathrm{He})$ is the difference in chemical potential, r_0 is the radius parameter characterizing the system and R $(^3\mathrm{H}/^3\mathrm{He})$ is the expected yield ratio. Using the values of T_{HHe} derived below and assuming normal density ($r_0=1.2$) we estimate the ratios to 4.4 for the ^{12}C induced reaction and 3.0 for the ^{64}Zn induced reaction. That these values are found to be well above the N/Z ratios of the composite system and reasonably close to the observed $t/^3$He ratios, is striking. Expansion and symmetry energy changes in the chemical potentials may also be playing a role in determining this ratio and this question is revisited in Sec. VI.

The values of the $t/^3$He ratio of Fig. 12(a) have been used to derive the N/Z ratio used in this analysis. This requires an approximation, either assuming P_0 to be identical for t and ^{3}He or alternatively assuming that the volumes at emission are the same for t and ^{3}He at a given V_{surf}. In the latter case Eq. (6), below, can be applied to determine the relative P_0 values, at least within the thermal model. Given the closeness of the binding energies of the two clusters these two approximations are almost equivalent. We have assumed identical P_0 values and substituted the $t/^3$He ratios for the N/Z ratios.

E. Experimental coalescence parameters P_0

In Fig. 13 values of P_0 derived from the observed yields of $Z=1$ and 2 clusters are presented for each system studied. For a given cluster species the four different systems have similar values of P_0 at high V_{surf}, supporting the idea of a similar emission mechanism for the higher energy particles in the different reactions studied. The P_0 values diminish with decreasing V_{surf}. This observed decrease of P_0 with decreasing surface velocity could reflect changes in the emitting system, a variation in the contributions from different emission sources or changes in the emission mechanism. A comparison of the data from the different reactions suggests that much of the decrease in P_0 observed at the lowest velocities in Fig. 13 results from the latter two causes, i.e., increasing contributions from late stage evaporative decay of the targetlike source or secondary decay from light fragments [8]. A coalescence approach is not valid at lower V_{surf} unless these contributions can be removed. To remove this contribution we have subtracted the targetlike source yields, obtained in the source fits, from the observed experimental yields. By this correction to the spectra we attempt to remove, as much as possible, secondary decay contributions in order to focus on the early evolution of the system. Values of P_0 determined from the corrected spectra are shown in Fig. 14. There we note that, for the heavier projectiles, P_0 decreases with decreasing surface velocity. Since P_0 is inversely related to the physical source size this indicates expansion in those systems.

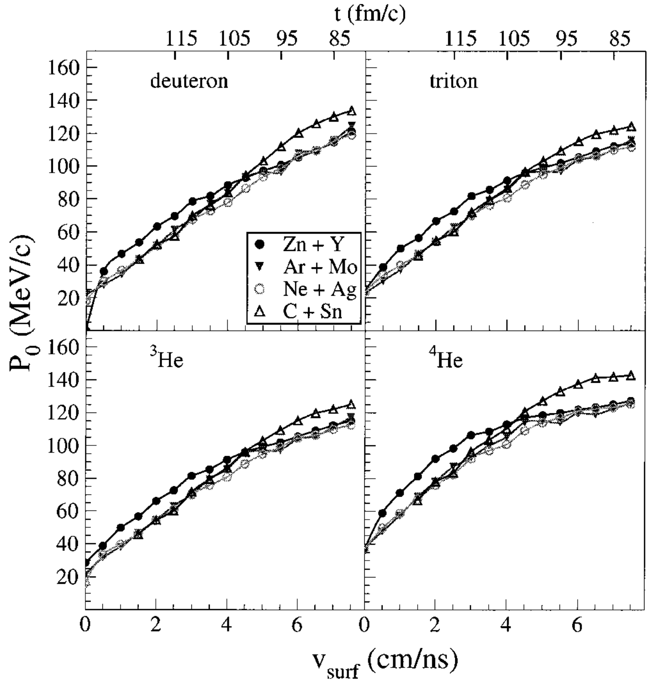

FIG. 13. Calculated values of the coalescence parameter P_0 as a function of surface velocity for p, d, t, ^{3}He, and ^{4}He clusters emitted in the four reactions studied. The entire yields observed at $\Theta_{\mathrm{lab}}=38-52°$ were employed in this calculation. Time scales derived from CHIMERA QMD model calculations are indicated at the top of the figure.

F. Determination of system size

Two different models were used to extract nuclear size information from the P_0 and T determinations, the density matrix model of Sato and Yazaki [11] and the thermal model of Mekjian [10]. Recall that the former is based on a sudden approximation while the latter assumes chemical and thermal equilibrium are achieved. At very high temperatures the dependence of the Mekjian model on temperature becomes

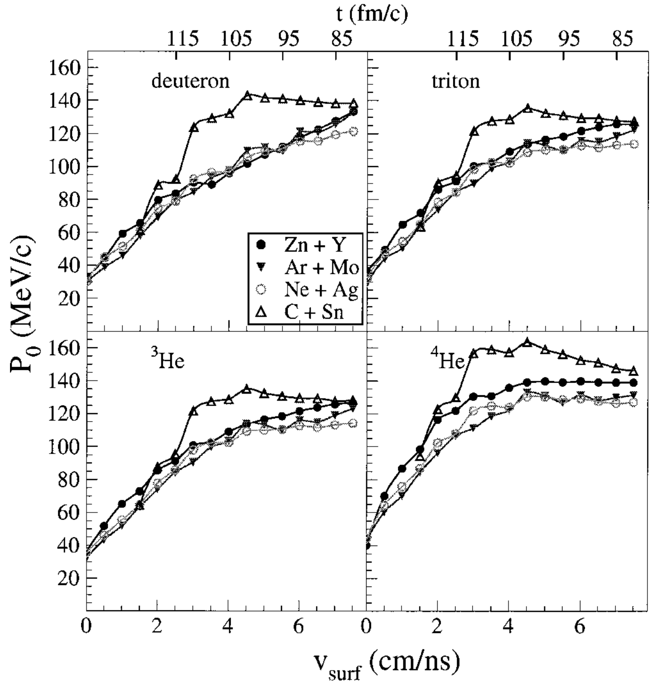

FIG. 14. Corrected values of the coalescence parameter P_0 as a function of surface velocity for *p, d, t,* ^{3}He, and ^{4}He clusters emitted in the four reactions studied. The contributions of to the ejectile spectra attributed to the TLF source have been subtracted from the experimental spectra at $\Theta_{lab}=38–52°$. Time scales derived from CHIMERA QMD model calculations are indicated at the top of the figure.

negligible and the two models are mathematically equivalent except for a cluster size correction which is included in the Sato-Yazaki model. At lower temperatures the Mekjian model is quite sensitive to the ratio of cluster binding energy to temperature.

G. The density matrix model

In the density matrix formalism of Sato and Yazaki [11] the size of the emitted cluster is explicitly taken into account in an attempt to refine the source size measurements:

$$\frac{d^3N_A}{d^3P_A}=R_{np}^{N}A^{5/2}\frac{2s+1}{2^A}\left(\frac{\hbar}{m_0}\right)^{A-1}\times\left((1+\beta_T\nu_A)\frac{4\pi\nu_A\nu}{\nu_A+\nu}\right)^{(3/2)(A-1)}\left(\frac{d^3N_p}{d^3P}\right)^{A}. \qquad (5)$$

Here R_{np} is the neutron to proton ratio of the coalescence source, ν and ν_A, respectively, characterize the spatial extent of the emitter and cluster wave functions (assumed to be Gaussian), and s is the spin of the cluster. The equivalent sharp radius of the emitter is then $\sqrt{5/2\nu}$. While this model does not assume thermal or chemical equilibrium it does contain a temperaturelike parameter $\beta_T=\hbar^2/(2m_0T)$ which characterizes the momentum distribution of the contributing particles at the time of emission. For this evaluation this parameter was derived by setting T equal to the Albergo temperature at the corresponding surface velocity. The sizes reported are the equivalent sharp cutoff radii of the emitting system.

H. Mekjian's thermal model

The thermal model which we have employed to derive sizes is the thermal coalescence model of Mekjian [10]. In this model thermal and chemical equilibrium are assumed. At equilibrium the relative yields of all species are determined. This model is consistent with many experimental observations [28], with a rapid equilibration of the emitting system [6,16,18,21], and with the apparent successes of several statistical models which have been applied to multifragmentation [3–5]. We note, in addition, that the Mekjian model and the model proposed by Albergo *et al.* to derive double isotope ratio temperatures [28] are, in fact, equivalent and the assumed validity of this model incorporating chemical equilibrium is implicit in all recent works which use such temperature measurements. Borderie *et al.* have recently provided evidence for the achievement of chemical equilibrium in violent collisions in this energy range [55].

It has been shown by Mekjian that under these assumptions there is a direct relationship between the volume in momentum space and the coordinate space volume of the emitting system [10]. In terms of the P_0 derived from Eq. (3) the relationship is

$$V=\left[\left(\frac{Z!N!A^3}{2^A}\right)(2s+1)e^{(E_0/T)}\right]^{1/(A-1)}\frac{3h^3}{4\pi P_0^3}, \qquad (6)$$

where Z, N, and A are the same as in Eq. (1), E_0 is the binding energy and s the spin of the emitted cluster and T is the temperature. Thus the radius can be derived from the observed P_0 and temperature values assuming a spherical source $R=(3V/4\pi)^{1/3}$.

I. Temperature determinations

For each model, deriving the size of the system from P_0 requires knowledge of the temperature. The observed spectral slopes are not appropriate estimates of the temperatures of the early emission spectra, as they reflect dynamic effects which produce hard and unreasonably high apparent temperatures. Indeed, the origin of these hard slopes (Fig. 6) is made clear by the transport model calculations. The observed spectra are convolutions of the spectra at different emission times and include high energy particles which are emitted prior to the achievement of thermal equilibrium.

To characterize the temperature at a particular emission time we have employed double isotope yield ratios. For a system at chemical and thermal equilibrium at a suitably low density, Albergo *et al.* [28] have shown that the temperature of the emitting system can be derived directly from the first chance emission double isotope yield ratios of two adjacent isotopes of two different elements. In a more recent work by Kolomiets *et al.* [56], essentially the same result is derived when only thermal equilibrium is assumed.

In the case of strong system evolution double isotope yield ratio temperatures derived from integrated yields are certainly suspect if the isotopes are in fact produced at very different times or by different mechanisms [8,30–32,38]. Selection of yields in a particular energy range, even when the energies are Coulomb corrected, may also lead to errors in temperature determinations if the isotopes are not in fact produced during the same time interval of the system evolution [8,29–32,38]. However, if the particles corresponding to particular emission times can be selected, for example using their velocities, and if secondary emission contributions are negligible, derivations of double isotope yield ratio temperatures as a function of particle velocity may allow us to follow the temperature evolution of the system. On the other hand, it should be clearly noted that the apparent temperature derived for the earliest stage may be only indicative of the particle momentum distribution at that emission time since the dynamic transport calculations indicate that the condition of thermal equilibrium is established only after some particle emission occurs.

We have derived the double isotope yield ratio temperature T_{HHe}, from the yields of *d*, *t*, ^{3}He, and ^{4}He particles as a function of V_{surf}. We note that for particles emitted from a single source of temperature T and having a volume Maxwellian spectrum $(E)^{1/2}e^{(-E/T)}$, the HHe double isotope yield ratio evaluated for particles of equal surface velocity is $\sqrt{8/9}$ times the ratio derived from either the integrated particle yields [28] or the yields at a given energy above the barrier [29]. Thus

$$T_{\mathrm{H\,He}}=\frac{14.3}{\ln[\sqrt{8/9}(1.59R_{v_{\mathrm{surf}}})]}, \tag{7}$$

where the constants 14.3 and 1.59 reflect binding energy, spin, masses and mass differences of the ejectiles and $R_{V\mathrm{surf}}=Y(d)Y(^4\mathrm{He})/Y(t)Y(^3\mathrm{He})$ with cluster yields Y taken at the same surface velocity.

In Fig. 12(b) we present the derived temperatures as a function of V_{surf}. The temperatures increase slowly with projectile mass and decrease with decreasing V_{surf}. They show some indications of a leveling in the 4–5 cm/ns range. At even lower V_{surf}, values of T_{HHe} in the 4–5 MeV range, similar to those spectral integrated values seen in other experiments are observed [29–32,35,56]. We take this latter observation, coupled with the changes in the t^3/He ratios seen in Fig. 12(a) as evidence for the limitations of the three source fitting process and that the spectra at these lower velocities still contain a contribution from late stage evaporation. Indeed these values are very similar to those calculated when the sequential evaporation code GEMINI [57] is used to simulate the deexcitation of the TLF source. As noted above, the three-source fits establish the fraction of the particle yield at a given V_{surf} which is assigned to either the TLF or *NN* sources. For a continuously evolving system the assignment of particles in the vicinity of the boundary is governed by the assumption of Maxwellian shapes for all source contributions. Thus subtraction of the TLF component yield may not be sufficient to remove some contribution from late stage evaporation. Since the spectra at the lowest velocities may still contain a residual contribution from late stage evaporation we do not attempt to extract emission system sizes for values of V_{surf} lower than 4 cm/ns which corresponds to ~ 105 fm/c in the QMD calculation.

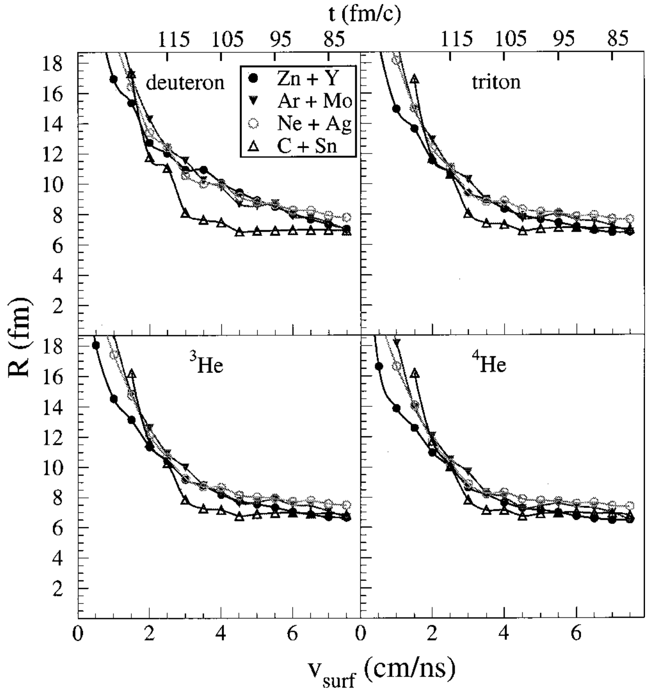

FIG. 15. Equivalent sharp radii derived from the Mekjian model. Radii for assumed spherical sources are presented as a function of surface velocity for *d*, *t*, ^{3}He, and ^{4}He clusters. The values of P_0 employed are those of Fig. 14. Time scales derived from CHIMERA QMD model calculations are indicated at the top of the figure.

J. System sizes

For both models, we present in Figs. 15 and 16, equivalent sharp cutoff radii for assumed spherical sources as derived from the P_0 values presented in Fig. 14. The size parameters are clearly different, reflecting differences in the models.

For each model, the sizes derived from the highest velocity particles show little dependence on projectile type and only for the lower energy ejectiles is a difference seen. The absolute values of the radii are larger for deuterons and smaller for α particles, possibly reflecting the very different binding and spatial extent of these clusters [11]. Such differences have been indicated in previous coalescence model studies [9–12]. That the differences persist in the density matrix model which attempts to take the cluster size into account is interesting and, if it does not result from simplifying assumptions implicit in the model, may imply some different freeze-out densities required for survival of different cluster species. However, other features of the dynamics might also explain this. For example, since the larger derived value of P_0 (and therefore smaller radius) is derived from the ratio of α multiplicity to nucleon multiplicity, it may be that

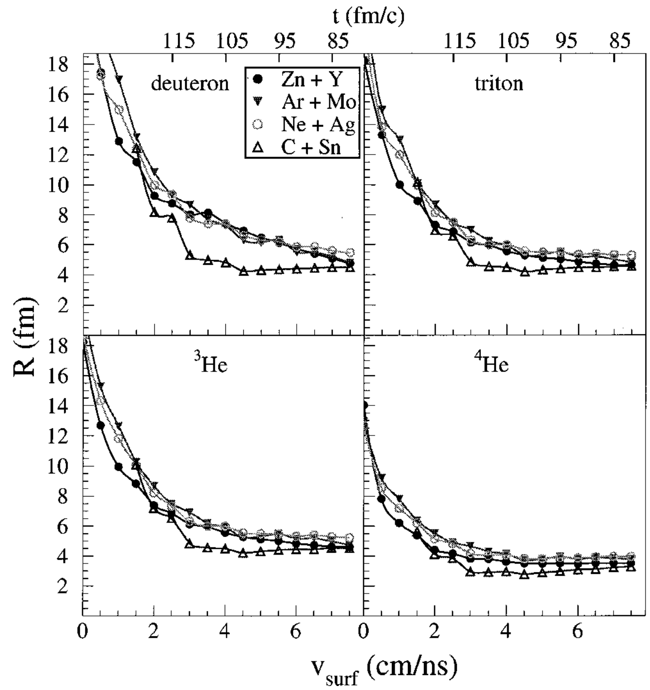

FIG. 16. Equivalent sharp radii derived from the Sato-Yazaki model. Radii for assumed spherical sources are presented as a function of surface velocity for *d, t,* ^{3}He, and ^{4}He clusters. The values of P_0 employed are those of Fig. 14. Time scales derived from CHIMERA QMD model calculations are indicated at the top of the figure.

there is an additional contribution to the α particle yield representing survival of initial correlations in the projectile or target [6,7]. The observation that the alpha particle spectrum seen in Fig. 6 has a high-energy slope which is softer than observed for the other $Z=1$ and 2 ejectiles, a difference made apparent in the slope temperature parameters for the *NN* source, is an indicator that some additional factors may be at play.

The SY model equivalent sharp radii are smaller than the radii of normal density nuclei in this mass range. This is true even if no correction is made for cluster size and apparently reflects the particular analytical formulation of the Sato-Yazaki model [11]. The values of thermal model radii at the highest values of V_{surf} are larger than those expected for the composite nuclei at normal density. This can be seen in Fig. 17 where the thermal model radii extracted from the triton data at $V_{\mathrm{surf}}=7$ cm/ns are plotted as a function of total entrance channel mass. For comparison lines corresponding to $R=1.2A^{1/3}$(solid) and $1.3A^{1/3}$ are shown. The former is a reasonable value for the sharp cutoff radii at normal density [58]. Also included in this plot are radii for heavier mass systems determined from a similar analysis for collisions of 47*A* MeV ^{12}C, ^{22}Ne, and ^{64}Zn projectiles with a ^{197}Au target [59].

Although subject to experimental uncertainties the thermal model results suggest that, at the time the early emitted particles leave the system, the size of the emitting nucleus is above normal. This is in qualitative agreement with the predictions of the QMD calculations for the early evolution of the system. As seen in Fig. 1, in the calculation the densities of the largest masses identifiable pass through normal density at a time ~ 50 fm/c, as the very first particles are emitted and are less than normal when subsequent particles leave. It is interesting to note that the results for the higher mass systems produced in reactions with Au indicate less deviation from the normal density for a given projectile type. This is consistent with less expansion at the emission time sampled.

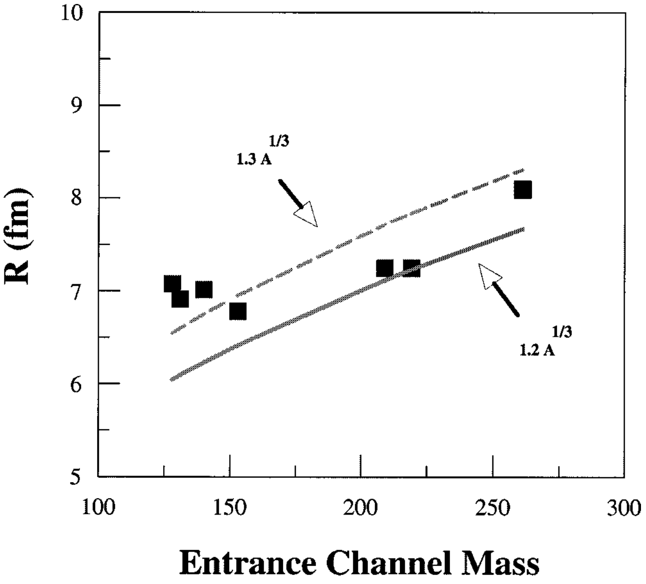

FIG. 17. Equivalent sharp radii derived from the Mekjian model for tritons at $V_{\mathrm{surf}}=7$ cm/ns. Radii are presented as a function of total entrance channel mass. For comparison radii calculated as $1.2A^{1/3}$ (solid line) and $1.3A^{1/3}$ (dashed line) are indicated.

For ^{12}C induced reactions the derived radii for the different particles indicate very little change of size during the particle emission phase. Progressively larger increases of the radii during particle emission are indicated for reactions with the heavier projectiles. This is indicated for triton emission in Fig. 18. The observed variation of P_0 with system at $V_{\mathrm{surf}}=7$ and 4 cm/ns, depicted in the top of the figure, leads to the variation of the radii shown in the center of the figure.

While the absolute values of the derived radii are different for the two models, for a given ejectile, the ratio $R(V_{\mathrm{surf}}=4\,\mathrm{cm/ns})/R(V_{\mathrm{surf}}=7\ \mathrm{cm/ns})$, a measure of the relative radius increase, is found to increase with projectile mass in a very similar fashion in the two models. This is shown in the bottom of Fig. 18 for *t* and ^{3}He emission. Although the relative variation observed is somewhat larger for deuteron emission and somewhat lower for α emission, the relative variations in radius as a function of V_{surf}, averaged over the four different ejectiles, are quite similar to those observed for *t* and ^{3}He emission. This is illustrated by the dashed lines in the bottom of Fig. 18. Since the derived absolute radii can be subject to systematic uncertainties both in the measurements and in the model assumptions, we choose, in the following section, to derive densities at freeze-out from the relative changes averaged over the four particles.

We end this section by asking how radii derived from the coalescence model analyses compare to results obtained ap-

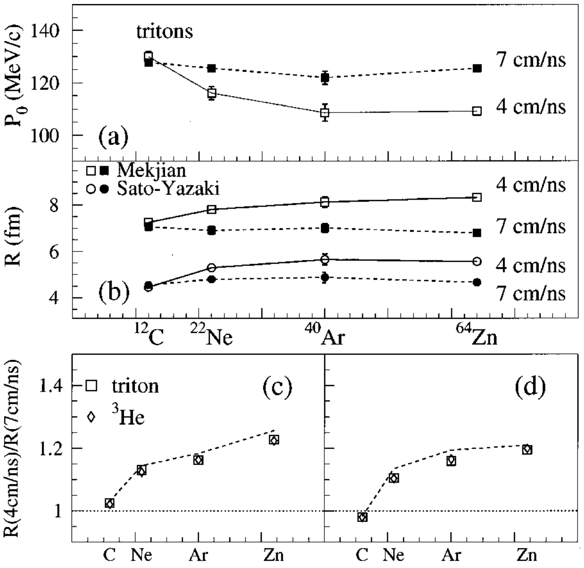

FIG. 18. P_0 values, radii, and relative radii at $V_{surf}=4$ and 7 cm/ns derived from the coalescence model analyses in all four systems studied. (a) P_0 values derived from triton data. (b) Radii derived from triton data. (c) The change in relative triton and ^{3}He radii observed in the Mekjian model. (d) The change in relative triton and ^{3}He radii observed in the Sato-Yazaki model. Dashed lines show the average changes for all four clusters.

plying the same type of analysis to a QMD transport model simulation. For this purpose we have employed the AMD-*V* model [60] to simulate the 47*A* MeV ^{64}Zn+^{89}Y reaction at $b=0$ to 3 fm and have then analyzed the results in the same manner as described here. The AMD-*V* model calculation shows similar early evolution to that calculated with CHIMERA but the AMD-*V* model includes antisymmetrization which has a particularly important effect in determining yields of $Z=1$ and 2 species. Recent studies have shown that the AMD-*V* model provides an excellent reproduction of most features of the data obtained in intermediate energy collisions, including isotopic yields, energy spectra and angular distributions [61,62]. In applying the coalescence calculation we demand internal consistency, taking into account the actual model binding energies and the spinless nature of the QMD particles. In Fig. 19 radii obtained by analyzing the AMD-*V* simulation at times up to 120 fm/*c* are shown for *d*, *t*, and ^{4}He (statistics for ^{3}He yields were too low for meaningful analysis). The trends are similar to those seen in our experiments. Since the calculation was stopped at 120 fm/*c* no indications of later secondary emission is seen. There are differences in absolute values. In the model, identification of clusters at short times was done by grouping all nucleons within 3 fm of each other. A change in this imposed criterion can affect the relative yields of different species and hence the absolute values of the radii.

K. Densities at freeze-out

To determine the average density associated with the system at $V_{surf}=4$ cm/ns, we first assumed that the highest velocity particles are emitted from an object of mass equal to

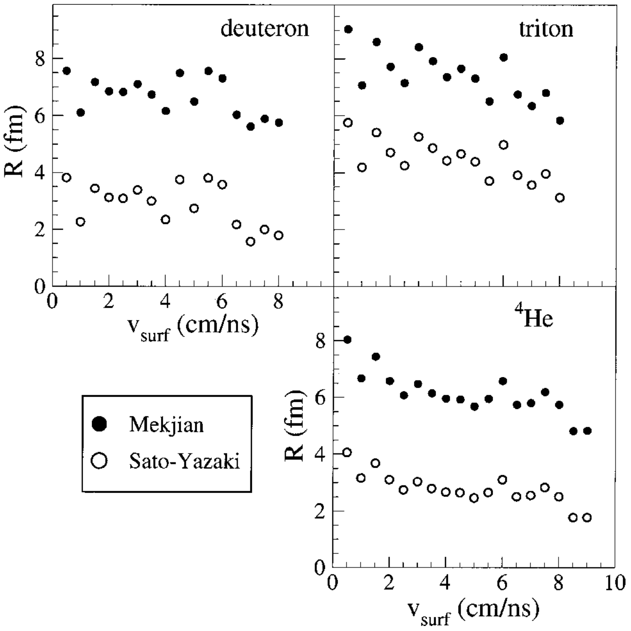

FIG. 19. Coalescence model calculations of radii derived from results of AMD-*V* calculations. Yield of clusters emitted up to 120 fm/*c* have been analyzed. Radii calculated from both the Mekjian [10] and Sato-Yazaki [11] formalisms are shown as a function of V_{surf}.

the sum of the masses of the target and projectile nuclei and of density equal to $0.90\rho_0$ (see Figs. 1,21). We then used the relative values of the radii derived from the *t*, ^{3}He, and ^{4}He data at 4 and 7 cm/ns and took the mass of the primary emitter at $V_{surf}=4$ cm/ns to be the mass remaining in the targetlike source. In that case the average density at 4 cm/ns may be written as

$$\frac{\rho}{\rho_0}=0.90\left(\frac{R_7}{R_4}\right)^3\left(\frac{A_4}{A_7}\right), \tag{8}$$

where *R*, the radius, and *A*, the mass, are taken at 4 and 7 cm/ns as indicated.

From the thermal model we find that the average densities sampled at $V_{surf}=4$ cm/ns are $0.81\rho_0$, $0.54\rho_0$, $0.45\rho_0$, and $0.36\rho_0$ for the ^{12}C, ^{22}Ne, ^{40}Ar, and ^{64}Zn induced reactions, respectively, with uncertainties of ±20% of these values. The corresponding values obtained using the Sato-Yazaki model are $0.94\rho_0$, $0.58\rho_0$, $0.45\rho_0$, and $0.38\rho_0$.

Our energy-density results are presented in Fig. 20. There we note that they are in very reasonable agreement with results of the CHIMERA QMD calculation when an equation of state with $K=200$ MeV is employed. For this soft equation of state the calculations indicate entry into the spinodal region [18–20] to the left of the dashed line $V_s^2=0$. A harder equation of state with $K=380$ MeV results in less expansion and poorer agreement with the experimental results. Refined measurements and coalescence analyses, including determinations of the impact parameter dependence of the cluster production might lead to a more precise determination of the incompressibility.

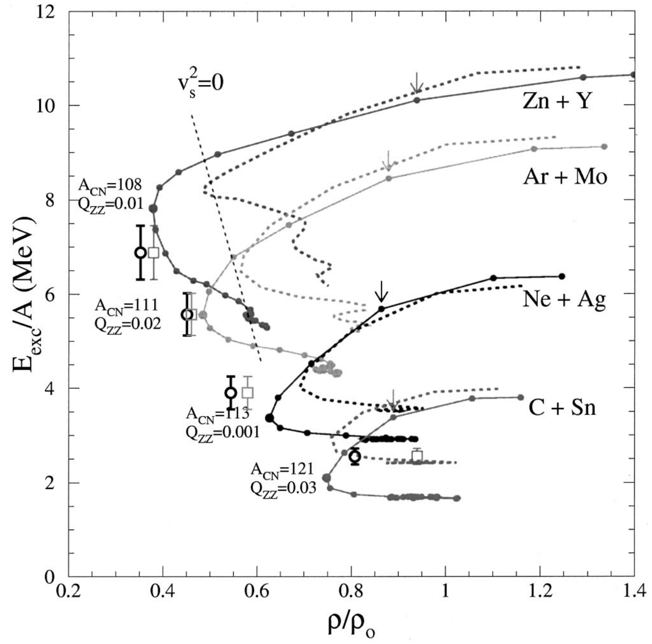

FIG. 20. Excitation energy-density values at freeze-out. The symbols represent the excitation-energy–density values, open circles, Mekjian model, open squares, Sato-Yazaki model, derived from coalescence model analyses of the light cluster emission. They are compared to CHIMERA QMD model trajectories in the excitation energy per nucleon-normalized density plane calculated for central collisions in the four different systems studied. Calculations for a soft $K=200$ MeV, equation of state are represented by solid lines. Calculations for a hard, $K=380$ MeV, equation of state are represented by thick dashed lines. The trajectories start at the time of maximum density. The small dots mark time increments of 10 fm/c. Arrows indicate the time of first emission of particles (near 50 fm/c after contact). Both times and Qzz values are indicated at the minimum calculated densities (large solid dots). To the left of the dashed line $V_s^2=0$, is the spinodal region [18–20].

L. Caloric curve

The double isotope yield ratio temperatures taken together with the excitation energies allow us to derive the nuclear caloric curve for a well defined low density nuclear source with $A\sim110$. We present in Fig. 21 the double isotope yield ratio temperatures at 4.0 cm/ns plotted against excitation energy. The results indicate a nearly flat caloric curve with $T\sim7$ MeV at excitation energies from 3.5 to 7 MeV per nucleon.

At the higher excitation energies, the double isotope yield ratio temperatures near 7 MeV indicated for the expanded low density systems are consistent with the limit suggested in our earlier work on the caloric curve for $A\sim125$ nuclei in which we found a temperature of 6.8 ± 0.5 MeV at 4.3 MeV/nucleon excitation energy [27]. The earlier results relied on slope measurements corrected for cascade effects. The agreement between that technique and the double-isotope ratio technique at excitation energies where the two measurements overlap is quite satisfying and gives us further confidence in our extraction of the early time temperatures in this work. The general shape of the caloric curve in Fig. 21 can then be understood as reflecting first, at lower excitations, primarily the washing out of shell effects and collectivity [63,64] and later, at higher energies, the expansion of the system.

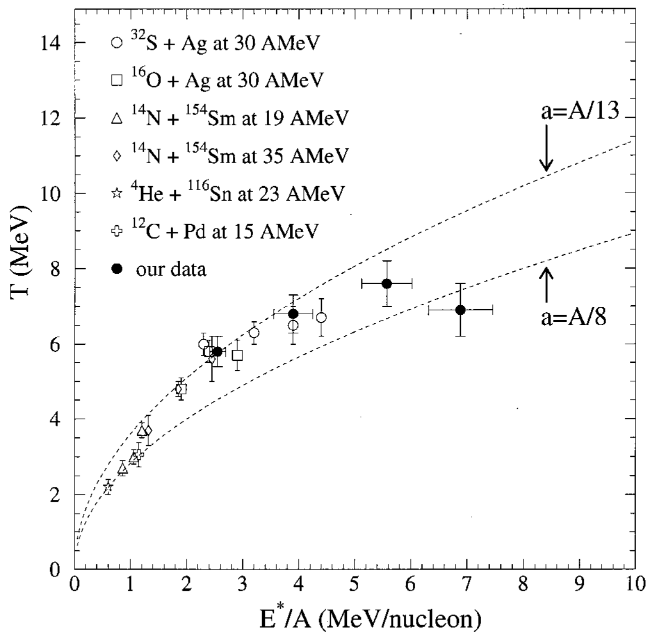

FIG. 21. Caloric curve for nuclei with $A\sim110$. Double isotope yield ratio temperatures derived in the present work are combined with results reported previously by Wada *et al.* obtained with a different technique [27]. Dashed lines indicate trends of a Fermi gas model calculation with two different choices of level density parameter.

The apparent limit near 7 MeV for this reasonably well-characterized mass region is in good accord with estimates made in a number of recent theoretical calculations [65–68]. This temperature is also significantly higher than many experimentally reported values for comparably excited systems [69–71]. In these latter works the double isotope ratio temperatures at comparable excitation energies, usually derived from time and energy integrated particle yields, are typically in the 5 MeV range. Only at low velocities (later times) where there is a possibility of inclusion of late stage evaporation cascade particles do our results approach such values. As pointed out, these lower velocity particles may not be completely removed by subtracting the TLF source since the evolution is more complicated than assumed in the simple three-source decomposition.

Recent Thomas-Fermi calculations also predict a lowering of the limiting temperature when radial flow is present [72]. It is interesting to note that the newly derived temperatures (at $V_{surf}=4.0$ cm/ns), presented in Fig. 21, initially rise with increasing projectile mass but may decrease again for the ^{64}Zn$+^{89}$Y reaction. Although the uncertainties in our measurements do not allow a definite conclusion to be made, such a behavior would be qualitatively consistent with systematics of radial flow measurements [73] from which we estimate a radial flow energy of ~0.3 MeV/nucleon for the ^{64}Zn induced reactions of this study and lower values for the lighter mass projectiles. This may suggest that the ^{22}Ne or ^{40}Ar induced collisions may lead to systems near the ‘‘balance point’’ [74].

In any case, it should be kept in mind that observed differences in caloric curves extracted from different reaction systems may reflect the particular dynamic evolution of the system being studied and great care must be taken to understand this dynamics. It should also be reemphasized that the evolution of the volume of the system is very important in determining the caloric curve [66,75]. Both classical and quantum molecular dynamics calculations lead to caloric curves similar to that observed here [65,76]. If a temperature limit of thermally equilibrated nuclei is reached, these calculations suggest that the system clusters and the nucleons with high kinetic energies stream out of the expanding system, creating a natural limit to the momentum distribution and to the excitation energy of the remaining nucleus over a wide transitional region [65,76].

VI. SUMMARY

In this work we have reported on the application of coalescence model techniques to the study of the dynamic evolution of highly excited expanding nuclear systems. For the reactions initiated by $47A$ MeV projectiles which we have studied we find that the more violent collisions produce increasing multiplicities of fragment and light particle emission as the projectile mass increases. The light ejectile spectra for the different systems exhibit strong similarities even though the deposited excitation energies differ greatly. Comparisons of the multiplicities and spectra of light charged particles emitted in the reactions with the four different projectiles indicate a common emission mechanism for those ejectiles associated with an intermediate velocity source even though the deposited excitation energies differ greatly. The ^{3}He spectra, in particular, appear to result predominately from this mechanism.

Self-consistent coalescence model analyses applied to the light cluster yields indicate increasing expansion of the emitting system with increasing projectile mass. At freeze-out, densities of the systems studied here range from just below normal density to $\sim 1/3$ of normal density. Masses of the expanded nuclei range from 102 to 116 u and excitation energies range from 2.6 to 6.9 MeV/nucleon. A caloric curve for expanded $A \sim 110$ nuclei exhibits a plateau at temperatures near 7 MeV. The plateau extends from ~ 3.5 to 6.9 MeV/nucleon excitation energy.

In the coalescence framework, measured values of the $t/^3$He ratio as a function of V_{surf} indicate ‘‘free nucleon density’’ ratios significantly higher than the N/Z ratios in the composite systems. Possible reasons for this are discussed in the paper. In particular, Eq. (4), which estimates the difference in chemical potential which occurs in a collision [54], was shown to lead to reasonable estimates of the $t/^3$He ratio when a radius parameter, $r_0 = 1.2$, corresponding to normal density is assumed. Since our systems are expanding and the chemical potential difference is sensitive to volume, it is interesting to ask what effect the expansion has on these estimates. This can be done by adopting in Eq. (4), for the different systems studied, r_0 values consistent with the determined densities. In this case the values of the $t/^3$He ratios decrease from 4.4 to 3.8 for the ^{12}C induced reaction and from 3.0 to 2.1 for the ^{64}Zn induced reaction. These values are in even better accord with those observed. This suggests again that the reaction dynamics is very important in determining this ratio.

Clearly we have relied on both data and theory to define this analysis. In our opinion, the very complexity of the disassembly problem demands this. Without this synergism a detailed understanding of the dynamics and of the disassembly mechanism will likely not be reached.

This work indicates that information on the space-time evolution of a system, complementary to that contained in HBT measurements, can be obtained in a relatively simple manner. It would clearly be interesting to make a direct comparison of the two techniques for some well-chosen cases. Recent HBT studies of multifragmenting systems at comparable excitation energies have been interpreted as indicating much lower freeze-out densities [77].

It would also be interesting to extend the application of the present coalescence techniques to the study of IMF emission in detailed experiments including both Z and A identification of the IMF which provide a sensitive probe of the degree of transparency and equilibration in the collision [78]. By clearly establishing the relative importance of different mechanisms of IMF formation it should be possible to explore the degree to which thermal and/or chemical equilibrium is achieved, the degree to which preexisting correlations are preserved, implying some transparency in the collisions. Indeed, although some recent works have suggested that IMFs are coalesced from a nucleon gas [51,79,80], several recent works exploring IMF production come to somewhat contradictory conclusions on this point [6,7,81]. More detailed investigations along the lines pursued here would allow a clearer picture of the degree to which the different species can be said to originate from either gaseous or liquid phases which might be present. Applying the techniques to systems of varying N/Z could provide a much clearer picture of isospin effects and the isospin dependence of symmetry energy [82–84].

ACKNOWLEDGMENTS

The authors appreciate very useful conversations with C-M. Ko, S. Shlomo, Y. Zheng, E. Gadioli, and E. Fabrici. This work was supported by The Robert A. Welch Foundation, the United States Department of Energy (Grant No. DE-FE05-86ER40256), and the Polish Scientific Research Committee (Grant No. 2 2392 91 02).

[1] E. Suraud, C. Gregoire, and B. Tamain, Prog. Part. Nucl. Phys. **23**, 357 (1989).

[2] B. Tamain and D. Durand, University of Caen Report No. LPCC 96-16, 1996 (unpublished), and references therein.

[3] D. H. E. Gross, Phys. Rep. **279**, 119 (1997).

[4] J. Bondorf *et al.*, Nucl. Phys. **A433**, 321 (1985).

[5] W. A. Friedman, Phys. Rev. C **42**, 667 (1990).

[6] P. B. Gossiaux and J. Aichelin, Phys. Rev. C **56**, 2109 (1997).

[7] J. P. Bondorf, D. Idier, and I. N. Mishustin, Phys. Lett. B **359**, 261 (1995).

[8] N. Marie *et al.*, The INDRA Collaboration, Phys. Rev. C **58**, 256 (1998).

[9] L. P. Csernai and J. I. Kapusta, Phys. Rep. **131**, 223 (1986).

[10] A. Z. Mekjian, Phys. Rev. C **17**, 1051 (1978); Phys. Rev. Lett. **38**, 640 (1977); Phys. Lett. **89B**, 177 (1980).

[11] H. Sato and K. Yazaki, Phys. Lett. **98B**, 153 (1981).

[12] T. C. Awes, G. Poggi, C. K. Gelbke, B. B. Back, B. G. Glagola, H. Breuer, and V. E. Viola, Jr., Phys. Rev. C **24**, 89 (1981).

[13] W. J. Llope, S. E. Pratt, N. Frazier, R. Pak, D. Craig, E. E. Gualtieri, S. A. Hannuschke, N. T. B. Stone, A. M. Vander Molen, G. D. Westfall, J. Yee, R. A. Lacey, J. Lauret, A. C. Mignerey, and D. E. Russ, Phys. Rev. C **52**, 2004 (1995).

[14] W. Bauer, C. K. Gelbke, and S. Pratt, Annu. Rev. Nucl. Part. Sci. **42**, 77 (1992).

[15] D. Ardouin, Int. J. Mod. Phys. E **6**, 391 (1997).

[16] J. Lukasik and Z. Majka, Acta Phys. Pol. B **24**, 1959 (1993).

[17] J. Cibor, J. Lukasik, and Z. Majka, Z. Phys. A **348**, 233 (1994).

[18] E. Suraud, M. Pi, P. Schuck, B. Remaud, F. Sebille, C. Gregoire, and F. Saint-Laurent, Phys. Lett. B **229**, 359 (1989).

[19] M. Colonna and P. Chomaz, Phys. Lett. B **436**, 1 (1998).

[20] G. Papp and W. Norenberg, Abst. Amer. Chem. Soc. **210**, 66 (1995).

[21] H. C. Chiang and J. Hufner, Nucl. Phys. **A349**, 466 (1980).

[22] I. Cervesato, E. Fabrici, E. Gadioli, E. Gadioli-Erba, and M. Galmarini, Phys. Rev. C **45**, 2369 (1992).

[23] J. B. Natowitz, S. Leray, R. Lucas, C. Ngo, E. Thomasi, and C. Volant, Z. Phys. A **325**, 467 (1986).

[24] Z. Y. He, G. M. Jin, Z. Y. Li, L. M. Duan, G. X. Dai, B. G. Zhang, H. Y. Wu, W. X. Wen, Y. J. Qi, and Q. Z. Luo, Phys. Rev. C **57**, 1824 (1998).

[25] C. J. Gelderlos, R. Sun, N. N. Ajitanand, J. M. Alexander, E. Bauge, A. Elmaani, T. Ethvignot, R. Lacey, M. E. Brandan, A. Giorni, D. Heuer, S. Kox, A. Lleres, A. Menchaca-Rocha, F. Merchez, S. D. Rebreyand, J. B. Viano, B. Chambon, B. Cheynis, D. Drain, and C. Pastor, Phys. Rev. C **52**, R2834 (1995).

[26] K. Hagel, D. Fabris, P. Gonthier, H. Ho, Y. Lou, Z. Majka, G. Mouchaty, M. N. Namboodiri, J. B. Natowitz, G. Nebbia, R. P. Schmitt, G. Viesti, R. Wada, and B. Wilkins, Nucl. Phys. **A486**, 429 (1988).

[27] R. Wada, D. Fabris, K. Hagel, G. Nebbia, Y. Lou, M. Gonin, J. B. Natowitz, R. Billerey, B. Cheynis, A. Demeyer, D. Drain, D. Guinet, C. Pastor, L. Vagneron, K. Zaid, J. Alarja, A. Giorni, D. Heuer, C. Morand, B. Viano, C. Mazur, C. Ngo, S. Leray, R. Lucas, M. Ribrag, and E. Tomasi, Phys. Rev. C **39**, 497 (1989).

[28] S. Albergo, S. Costa, E. Costanzo, and A. Rubbino, Nuovo Cimento A **89**, 1 (1985).

[29] H. Xi, M. J. Huang, W. G. Lynch, S. J. Gaff, C. K. Gelbke, T. Glasmacher, G. J. Kunde, L. Martin, C. P. Montoya, S. Pratt, M. B. Tsang, W. A. Friedman, P. M. Milazzo, M. Azzano, G. V. Margagliotti, R. Rui, G. Vannini, N. Colonna, L. Celano, G. Tagliente, M. D'Agostino, M. Bruno, M. L. Fiandri, F. Gramegna, A. Ferrero, I. Iori, A. Moroni, F. Petruzzelli, and P. F. Mastinu, Phys. Rev. C **57**, R462 (1998).

[30] G. J. Kunde, S. Gaff, C. K. Gelbke, T. Glasmacher, M. J. Huang, R. Lemmon, W. G. Lynch, L. Manduci, L. Martin, M. B. Tsang, W. A. Friedman, J. Dempsey, R. J. Charity, L. G. Sobotka, D. K. Agnihotri, B. Djerroud, W. U. Schroeder, W. Skulski, and J. Toke, Phys. Lett. B **416**, 56 (1998).

[31] H. F. Xi, G. J. Kunde, O. Bjarki, C. K. Gelbke, R. C. Lemmon, W. G. Lynch, D. Magestro, R. Popescu, R. Shomin, M. B. Tsang, A. M. Vandermolen, G. D. Westfall, G. Imme, V. Maddalena, C. Nociforo, G. Raciti, G. Riccobene, F. P. Romano, A. Saija, C. Sfienti, S. Fritz, C. Grob, T. Odeh, C. Schwarz, A. Nadasen, D. Sisan, and K. A. G. Rao, Phys. Rev. C **58**, R2636 (1998).

[32] V. E. Viola, K. Kwiatkowski, and W. A. Friedman, Phys. Rev. C **59**, 2660 (1999).

[33] J. Cibor, R. Wada, K. Hagel, M. Lundardon, N. Marie, R. Alfaro, W.Q. Shen, B. Xiao, Y. Zhao, J. Li, B.A. Li, M. Murray, J.B. Natowitz, Z. Majka and P. Staszel, Phys. Lett. B **473**, 29 (2000); J. Cibor, R. Wada, K. Hagel, N. Marie, B. Xiao, Y. Zhao, Z. Majka, J. Li, P. Staszel, M. Murray, and J.B. Natowitz, *Proceedings of the Workshop on Nuclear Matter in Different Phases and Transitions*, edited by J-P Blaizot, X. Campi, and M. Ploszajczak (Les Houches, Paris, 1998), p. 479.

[34] R. P. Schmitt, L. Cooke, G. Derrig, D. Fabris, B. Hurst, J. B. Natowitz, G. Nebbia, D. O'Kelly, B. Srivastava, B. Turmel, D. Utley, H. Utsonomiya, and R. Wada, Nucl. Instrum. Methods Phys. Res. A **354**, 487 (1995).

[35] R. Wada, R. Tezkratt, K. Hagel, F. Haddad, A. Kolomiets, Y. Lou, J. Li, M. Shimooka, S. Shlomo, D. Utley, B. Xiao, N. Mdeiwayeh, J. B. Natowitz, Z. Majka, J. Cibor, T. Kozik, and Z. Sosin, Phys. Rev. C **55**, 227 (1997).

[36] A. M. Poskanzer, G. W. Butler, and E. K. Hyde, Phys. Rev. C **3**, 882 (1971).

[37] H. H. Gutbrod, A. M. Poskanzer, and H. G. Ritter, Rep. Prog. Phys. **52**, 1267 (1989).

[38] N. Marie *et al.*, The INDRA Collaboration, Phys. Lett. B **391**, 15 (1997).

[39] R. Bougault *et al.*, in Proceedings of XXXV International Winter Meeting on Nuclear Physics, Bormio, Italy, edited by I. Iori, 1997 (unpublished).

[40] T. C. Awes, G. Poggi, S. Saini, C. K. Gelbke, R. Legrain, and G. D. Westfall, Phys. Lett. **103B**, 417 (1981).

[41] D. Prindle, A. Elmaani, C. Hyde-Wright, W. Jiang, A. A. Sonzogni, R. Vandenbosch, D. Bowman, G. Cron, P. Danielewicz, J. Dinius, W. Hsi, W. G. Lynch, C. Montoya, G. Peaslee, C. Schwarz, M. B. Tsang, C. Williams, R. T. de Souza, D. Fox, and T. Moore, Phys. Rev. C **57**, 1305 (1998).

[42] V. E. Viola, B. B. Back, K. L. Wolf, T. C. Awes, C. K. Gelbke, and H. Breuer, Phys. Rev. C **26**, 178 (1982).

[43] S. Leray, J. Phys. C **4**, 275 (1986).

[44] D. H. Boal, Phys. Rev. C **25**, 3068 (1982).

[45] M.-C. Lemaire, S. Nagamiya, S. Schnetzer, H. Steiner, and I. Tanihata, Phys. Lett. **85B**, 38 (1979).

[46] J. Barrette, R. Bellwied, P. Braun-Munzinger, W. E. Cleland,

T. M. Cormier, G. David, J. Dee, G. E. Diebold, O. Dietzsch, J. V. Germani, S. Gilbert, S. V. Greene, J. R. Hall, T. K. Hemmick, N. Herrmann, B. Hong, K. Jayananda, D. Kraus, B. S. Kumar, R. Lacasse, D. Lissauer, W. J. Llope, T. W. Ludlam, S. McCorkle, R. Majka, S. K. Mark, J. T. Mitchell, M. Muthuswamy, E. O'Brien, C. Pruneau, F. S. Rotondo, J. Sandweiss, N. C. daSilva, U. Sonnadara, J. Stachel, H. Takai, E. M. Takagui, T. G. Throwe, D. Wolfe, C. L. Woody, N. Xu, Y. Zhang, Z. Zhang, and C. Zou, The E814 Collaboration, Phys. Rev. C **50**, 1077 (1994).
[47] R. Scheibl and U. Heinz, Phys. Rev. C **59**, 1585 (1999).
[48] J. Cibor, A. Bonasera, J.B. Natowitz, R. Wada, K. Hagel, M. Murray, and T. Keutgen, Isospin Physics in Heavy-Ion Collisions at Intermediate Energies, edited by B. A. Li and W. U. Schroeder (Nova Science, in press).
[49] M. Belkacem, V. Latora, and A. Bonasera, Phys. Rev. C **52**, 271 (1995).
[50] L. G. Sobotka, J. F. Dempsey, R. J. Charity, and P. Danielewicz, Phys. Rev. C **55**, 2109 (1997).
[51] H. S. Xu, M. B. Tsang, T. X. Liu, X. D. Liu, W. G. Lynch, W. P. Tan, G. Verde, A. Vandermolen, A. Wagner, H. F. Xi, C. K. Gelbke, L. Beaulieu, B. Davin, Y. Larochelle, T. Lefort, R. T. de Souza, R. Yanez, V. Viola, R. J. Charity, and L. G. Sobotka, Michigan State Report No. MSUCL-1137; NSCL Report No. 5526, 1999.
[52] H. Muller and B. Serot, Phys. Rev. C **52**, 2072 (1995).
[53] V. Baran, M. Colonna, M. Di Toro, and A. B. Larioinov, Nucl. Phys. **A632**, 287 (1998).
[54] A. Bonasera and G. F. Bertsch, Phys. Lett. B **195**, 521 (1987).
[55] B. Borderie, F. Gulminelli, M. F. Rivet, L. Tassan-Got, M. Assenard, G. Auger, F. Bocage, R. Bougault, R. Brou, P. Buchet, J. Colin, R. Dayras, A. Demeyer, J. D. Frankland, E. Galichet, E. Genouin-Duhamel, E. Gerlic, M. Germain, D. Guinet, P. Lautesse, J. L. Laville, J. F. Lecolley, T. Lefort, R. Legrain, N. Le Neindre, M. Louvel, A. M. Maskay, L. Nalpas, A. D. Nguyen, M. Parlog, E. Plagnoll, A. Rahmani, T. Reposeur, E. Rosato, F. Saint-Laurent, S. Salou, J. C. Steckmeyer, M. Stern, G. Tabacaru, B. Tamain, O. Tirel, D. Vintache, and C. Volant, Eur. Phys. J. A **6**, 197 (1999).
[56] A. Kolomiets *et al.*, Phys. Rev. C **55**, 1376 (1997).
[57] R. J. Charity *et al.*, Nucl. Phys. **A483**, 371 (1988).
[58] M. A. Preston, *Physics of the Nucleus* (Addison-Wesley, Reading, MA, 1962).
[59] M. Lunardon *et al.* (unpublished).
[60] A. Ono and H. Horiuchi, Phys. Rev. C **53**, 2958 (1996).
[61] A. Ono, Phys. Rev. C **59**, 853 (1999).
[62] R. Wada, K. Hagel, J. Cibor, M. Gonin, Th. Keutgen, M. Murray, J. B. Natowitz, A. Ono, J. C. Steckmeyer, A. Kerambrum, J. C. Angelique, A. Auger, G. Bizard, R. Brou, C. Cabot, E. Crema, D. Cussol, D. Durand, Y. El-Masri, P. Eudes, Z. Y. He, S. C. Jeong, C. Lebrun, J. P. Patry, A. Peghaire, J. Peter, R. Regimbart, E. Rosato, F. Saint-Laurent, B. Tamain, and E. Vient, Phys. Rev. C **62**, 034601 (2000).
[63] S. Shlomo and J. B. Natowitz, Phys. Rev. C **44**, 2878 (1991).
[64] J. N. De, S. Shlomo, and S. Samaddar, Phys. Rev. C **57**, 1398 (1998).
[65] F. Gulminelli and D. Durand, Nucl. Phys. **A615**, 117 (1997).
[66] Y. Sugawa and H. Horiuchi, Phys. Rev. C **60**, 064607 (1999).
[67] P. Bonche *et al.*, Nucl. Phys. **A427**, 278 (1984).
[68] H. Q. Song and R. K. Su, Phys. Rev. C **44**, 2505 (1991).
[69] J. Pochodzalla *et al.*, Phys. Rev. Lett. **75**, 1040 (1995).
[70] J. A. Hauger, P. Warren, S. Albergo, F. Bieser, F. P. Brady, Z. Caccia, D. A. Cebra, A. D. Chacon, J. L. Chance, Y. Choi, S. Costa, J. B. Elliott, M. L. Gilkes, A. S. Hirsch, E. L. Hjort, A. Insolia, M. Justice, D. Keane, J. C. Kintner, V. Lindenstruth, M. A. Lisa, H. S. Matis, M. McMahan, C. McParland, W. F. J. Muller, D. L. Olson, M. D. Partlan, N. T. Porile, R. Potenza, G. Rai, J. Rasmussen, H. G. Ritter, J. Romanski, J. L. Romero, G. V. Russo, H. Sann, R. P. Scharenberg, A. Scott, Y. Shao, B. K. Srivastava, T. J. M. Symons, M. Tincknell, C. Tuve, S. Wang, H. H. Wieman, T. Wienold, and K. Wolf, EOS Collaboration, Phys. Rev. C **57**, 764 (1998).
[71] Y. G. Ma *et al.*, Phys. Lett. B **390**, 41 (1997).
[72] J. N. De, S. K. Samaddar, and S. Shlomo, Nucl. Phys. **A630**, 192c (1998).
[73] M.-F. Rivet, GANIL Report No. 97-08 (1997).
[74] S. Pratt, C. Montoya, and F. Ronning, Phys. Lett. B **349**, 261 (1995).
[75] L. G. Moretto, R. Ghetti, L. Phair, K. Tso, and G. J. Wozniak, Phys. Rev. Lett. **76**, 2822 (1996).
[76] A. Strachan and C. O. Dorso, Phys. Rev. C **58**, R632 (1998); **59**, 285 (1999).
[77] W. Trautmann for the ALADIN Collaboration, *Advances in Nuclear Dynamics 4*, edited by W. Bauer and H. G. Ritter (Plenum, New York, 1998), p. 349.
[78] H. Johnston, T. White, J. Winger, D. Rowland, B. Hurst, F. Gimeno-Nogues, D. O'Kelly, and S. J. Yennello, Phys. Lett. B **371**, 186 (1996).
[79] B. V. Jacak, D. Fox, and G. D. Westfall, Phys. Rev. C **31**, 704 (1985).
[80] M. Cavinato, E. Fabrici, E. Gadioli, E. G. Erba, M. Galmarini, and A. Gritti, Z. Phys. A **347**, 237 (1994).
[81] E. Colin, R. Sun, N. N. Ajitanand, John M. Alexander, M. A. Barton, P. A. DeYoung, A. Elmaani, C. J. Gelderloos, E. E. Gualtieri, D. Guinet, S. Hannuschke, J. A. Jasma, L. Kowlaski, R. A. Lacey, J. Lauret, E. Norbeck, R. Pak, G. F. Peaslee, M. Stern, N. T. B. Stone, S. D. Sundbeck, A. M. Vander Molen, G. D. Westfall, and J. Yee, Phys. Rev. C **57**, R1032 (1998).
[82] B. A. Li and S. J. Yennello, Phys. Rev. C **52**, R1746 (1995).
[83] B-A. Li, C-M. Ko, and W. Bauer, Int. J. Mod. Phys. E **7**, 147 (1998).
[84] C. H. Lee, T. T. S. Kuo, G. Q. Li, and G. E. Brown, Phys. Rev. C **57**, 3488 (1998).